The Abdus Salam International Centre for Theoretical Physics

United Nations Educational, Scientific and Cultural Organization

IAEA International Atomic Energy Agency

1932-20

Winter College on Micro and Nano Photonics for Life Sciences

11 - 22 February 2008

Applications of photonic crystals

Marco CENTINI

Università degli Studi di Roma 'La Sapienza'
Rome, Italy

The Abdus Salam
International Centre for Theoretical Physics

United Nations
Educational, Scientific
and Cultural Organization

International Atomic
Energy Agency

Winter College on Micro and Nano Photonics for Life Sciences

(11-22 February 2008)

Applications of Photonic Crystals:

Scraping the surface…

M.Centini
Universita' di Roma, "La Sapienza", Roma, Italy

Outline

- Using Photonic Crystals properties for integrated sources and devices;

- Tailored DOS, Control of Spontaneous emission, Ph.C.microcavities;

- Photonic Crystal Biosensors: a few examples;

- Photonic crystal fibers and applications;

- Nonlinear effects enhancement, SHG and parametric fluorescence

Bulk Photonic crystals properties

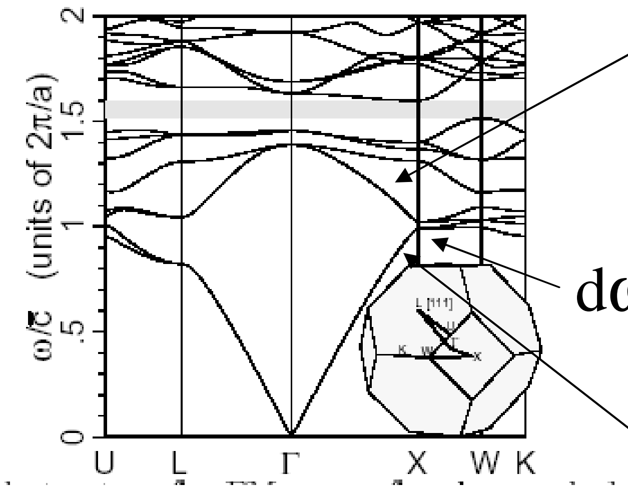

Complex band structure

backwards slope:

negative refraction

dω/d*k* → 0: slow light

(e.g. DFB lasers)

strong curvature:

super-prisms, …

(+ negative refraction)

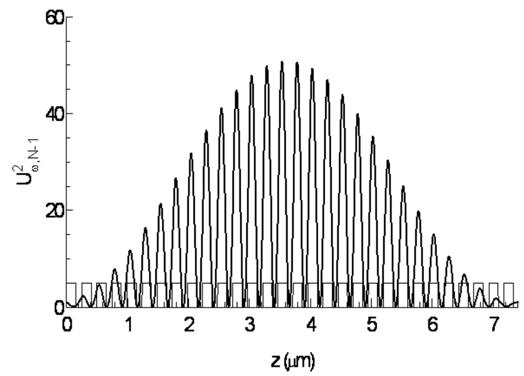

Internal field enhancement

- Low threshold lasing
- Enhanced nonlinear optical effects

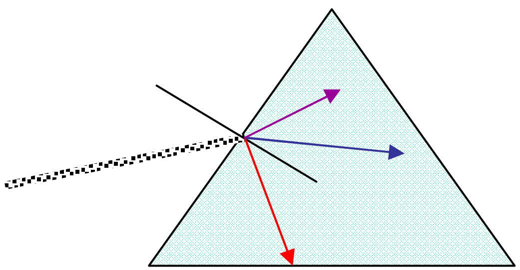

Spatial dispersion (Superprism effect)

- Negative refraction
- Large angle deflection 500x
- Self-collimation

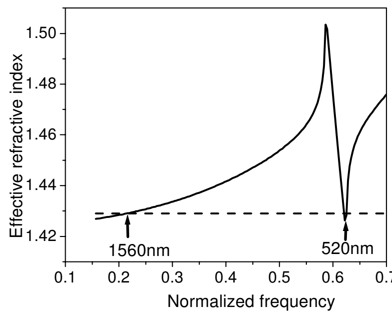

Dispersive refractive index dispersion

- Control of light propagation
- Phase-matching for harmonic generation

Control of Electromagnetic Waves

Optical Microcavities: High Q and small V_{eff}

The interaction of light and matter can be dramatically altered by the presence of a microcavity;

The degree to which it is affected is a function of the photon lifetime in the cavity ($Q=\omega\tau_{ph}$) and the spatial localization (V_{eff}).

Some important processes depending on Q and V_{eff} include:

- **Enhanced spontaneous emission (Purcell factor) ~ Q/V_{eff} ;**

- **Strong atom-photon coupling in cavity QED ~ $Q/(V_{eff})^{1/2}$;**

- **Raman lasing threshold ~ V_{eff}/Q^2 ;**

- **Second harmonic generation, Nonlinear parametric interactions**

- **Single molecule fluorescence detection**

- **Biomolecular sensing**

K. J. Vahala, "Optical microcavities", Nature, vol. 424, No. 6950, August 2003

S. Noda et al. Nature Photonics Vol 1 August 2007

Electromagnetic Density of States for a finite-size three-dimensional structure

Starting from the power emitted by an electric dipole of dipole moment p_0 oriented along $\hat{x}$ in a 3D system:

$$\overline{W}_{\text{emitted}}(\vec{r}_0) = -\frac{\omega^3 \mu_0 |\vec{p}_0|^2}{2} \mathrm{Im}[G_{\omega,\hat{x}\hat{x}}(\vec{r}_0, \vec{r}_0)],$$

For a dipole emitting in the free space:

$$\overline{W}_{\text{emitted,free space}} = \frac{\omega^4 \mu_0 |\vec{p}_0|^2}{12\pi c}.$$

$$\rho(\omega) = \frac{\omega^2}{\pi^2 c^3};$$

Spatial average over the volume of the open system

Local DOS

$$\rho_\omega(\vec{r}) \equiv \rho_{\omega,\text{free space}} \frac{\overline{W}_{\text{emitted}}(\vec{r})}{\overline{W}_{\text{emitted,free space}}} = -\frac{6\pi c}{\omega} \rho_{\omega,\text{free space}} \mathrm{Im}[G_{\omega,\hat{x}\hat{x}}(\vec{r}, \vec{r})].$$

DOS

$$\rho_\omega \equiv \rho_{\omega,\text{free space}} \frac{\langle \overline{W}_{\text{emitted}}(\vec{r}) \rangle}{\overline{W}_{\text{emitted,free space}}} = -\frac{6\pi c}{\omega} \rho_{\omega,\text{free space}} \langle \mathrm{Im}[G_{\omega,\hat{x}\hat{x}}(\vec{r}, \vec{r})] \rangle,$$

D'Aguanno et al. PHYSICAL REVIEW E 69, 057601 (2004)

Spontaneous-emission enhancement/suppression

Fermi's golden rule states that the single atomic dipole rate of transition *W* from an excited state to a lower state through emission of a photon of frequency ω may be written as:

DOS

$$W_{\omega}=\frac{2\pi}{\hbar}\rho_{\omega}|\langle f|H_{\rm int}|i\rangle|^{2},$$

H_{int}=**μ•E** is the interaction Hamiltonian that couples the dipole moment operator μ to the electric field **E**, and |i> and |f> are the initial and final states of the dipole-field system

The rate of this transition is determined by the photonic density of states and the electric-field strength at the position of the emitter.

Enhanced spontaneous emission

Suppression of spontaneous emission

1D DOS

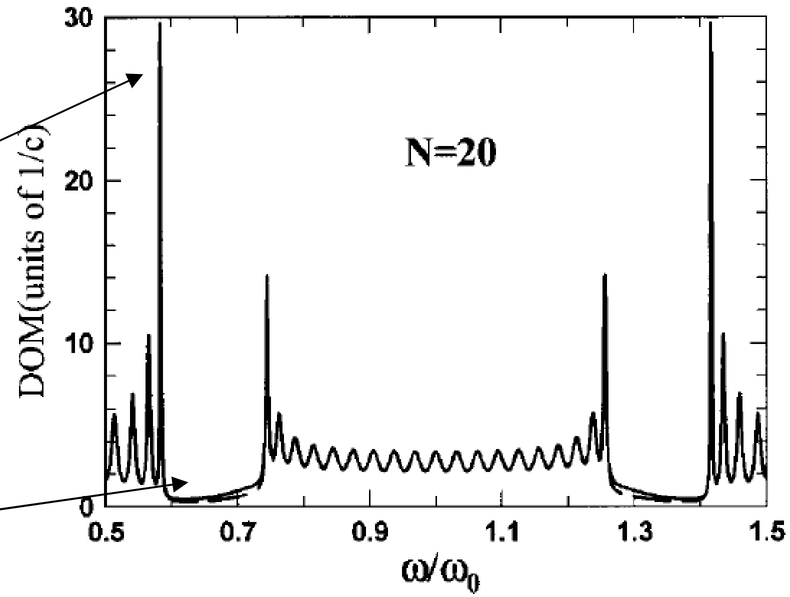

SUSUMU NODA*, MASAYUKI FUJITA AND TAKASHI ASANO
Department of Electronic Science and Engineering, Kyoto University, Katsura, Nishikyo-Ku, Kyoto 615-8510, Japan

nature photonics | VOL 1 | AUGUST 2007 | www.nature.com/naturephotonics

Spontaneous-emission control by photonic crystals and nanocavities

We describe the recent experimental progress in the control of spontaneous emission by manipulating optical modes with photonic crystals. It has been clearly demonstrated that the spontaneous emission from light emitters embedded in photonic crystals can be suppressed by the so-called photonic bandgap, whereas the emission efficiency in the direction where optical modes exist can be enhanced. Also, when an artificial defect is introduced into the photonic crystal, a photonic nanocavity is produced that can interact with light emitters. Cavity quality factors, or Q factors, of up to 2 million have been realized while maintaining very small mode volumes, and both spontaneous-emission modification (the Purcell effect) and strong-coupling phenomena have been demonstrated. The use of photonic crystals and nanocavities to manipulate spontaneous emission will contribute to the evolution of a variety of applications, including illumination, display, optical communication, solar energy and even quantum-information systems.

Spontaneous emission (SE) occurs when an emitter relaxes from an excited state to its ground state by photon emission into an optical mode that is not occupied by other photons.

Manipulation of SE, can be obtained by controlling the number of optical modes and their spatial distribution relative to the emitter.

2D example

GaInAsP 2D PC slab with a single quantum-well (QW) light-emitting layer

Thin freestanding semiconductor slab structure:
semiconductor core (n ~ 3)
air cladding (n=1)

the overall SE rate is expected to decrease substantially as a result of the inhibition of optical modes in all 2D directions by the 2D PBG effect, whereas the emission efficiency in the direction normal to the crystal (in which the 2D PBG effect does not appear) is expected to increase.

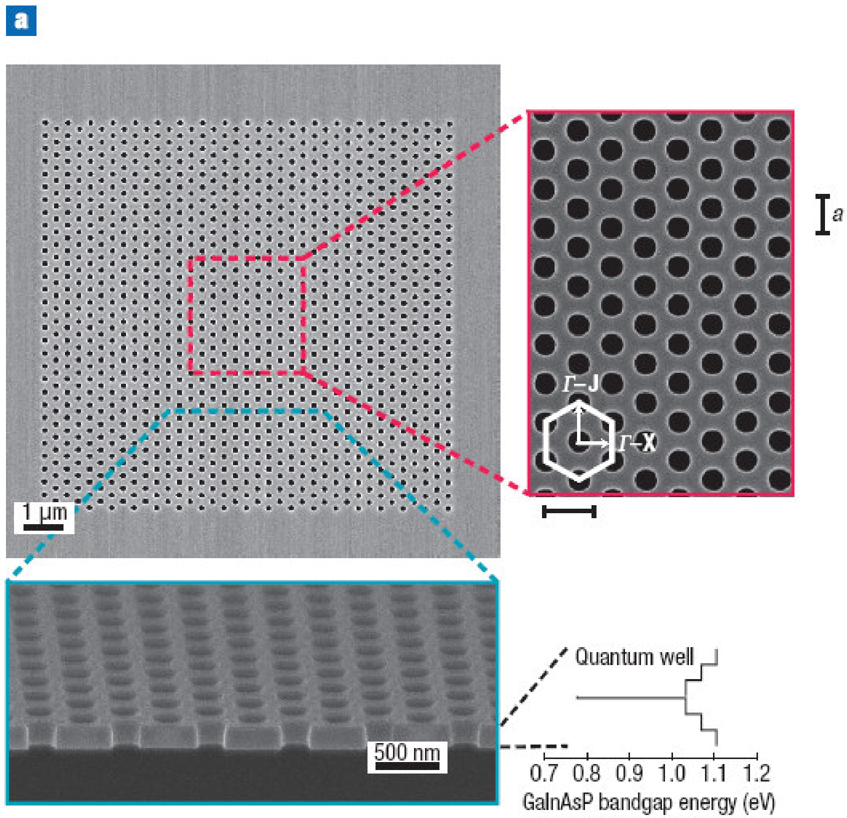

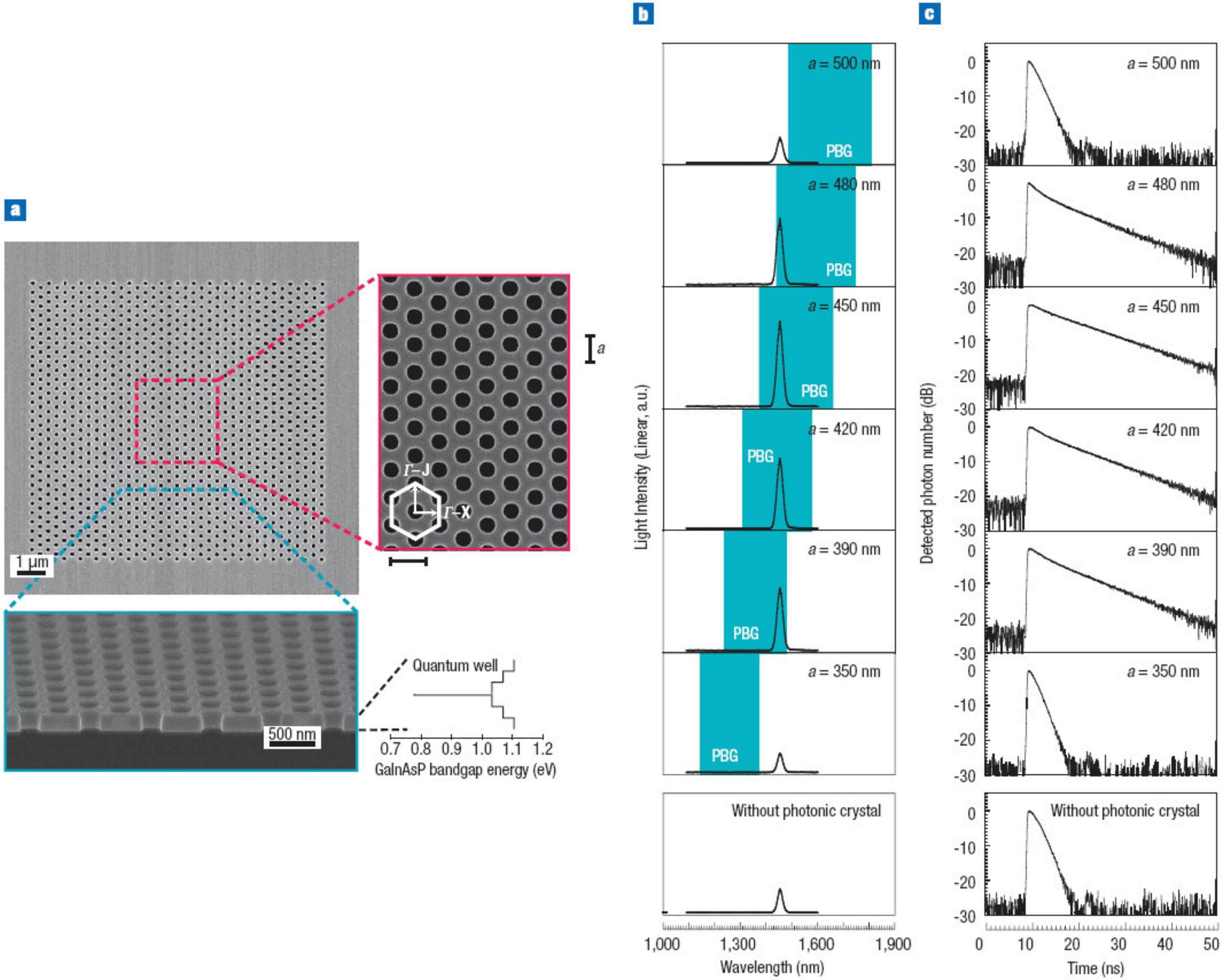

Figure 3 Experimental results of SE control by 2D PC slab with a QW emitter. **a**, An SEM image of the slab. Γ–J and Γ–X represent the directions of the triangular lattice 2D photonic crystal in which photons propagate. **b**, Time-integrated emission spectra for various lattice constants. The blue shading denotes the PBG region. **c**, Time-resolved PL measurement for various samples. When the SE spectrum is within the PBG region, the emission lifetime increases by a factor of five compared with that outside the PBG region or without a PC structure. A corresponding increase in the light-emission efficiency in the vertical mode is clearly observed in the PBG region in **b**. Reproduced with permission from ref. 11. Copyright (2005) AAAS.

Photonic nanocavity, SE coupled to the nanocavity mode.
the emission rate of the cavity mode can be significantly enhanced by a factor of Q/V, by means of the Purcell effect.

the modal volume V *can be* very small (the order of a cubic wavelength).
Increasing Q while keeping a small V *is not easy*, as the radiation loss increases in inverse proportion to the cavity size.

L3 Cavity, 3 holes are missing

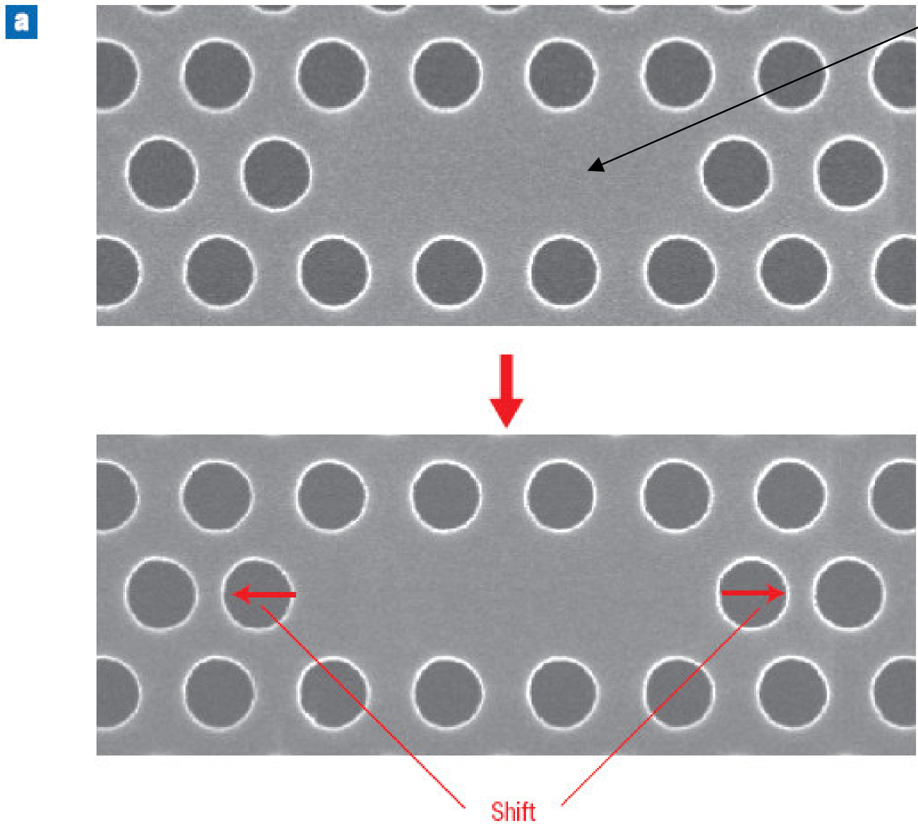

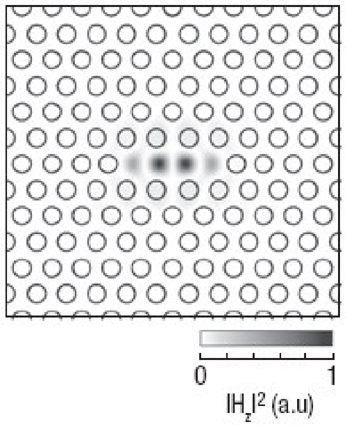

Q=45000 with a cavity volume $V = 0.69(\lambda/n)3$

Basic idea to obtain minimum losses in the vertical direction

Akahane et al, Nature **425, 944-947 (30 October 2003)**

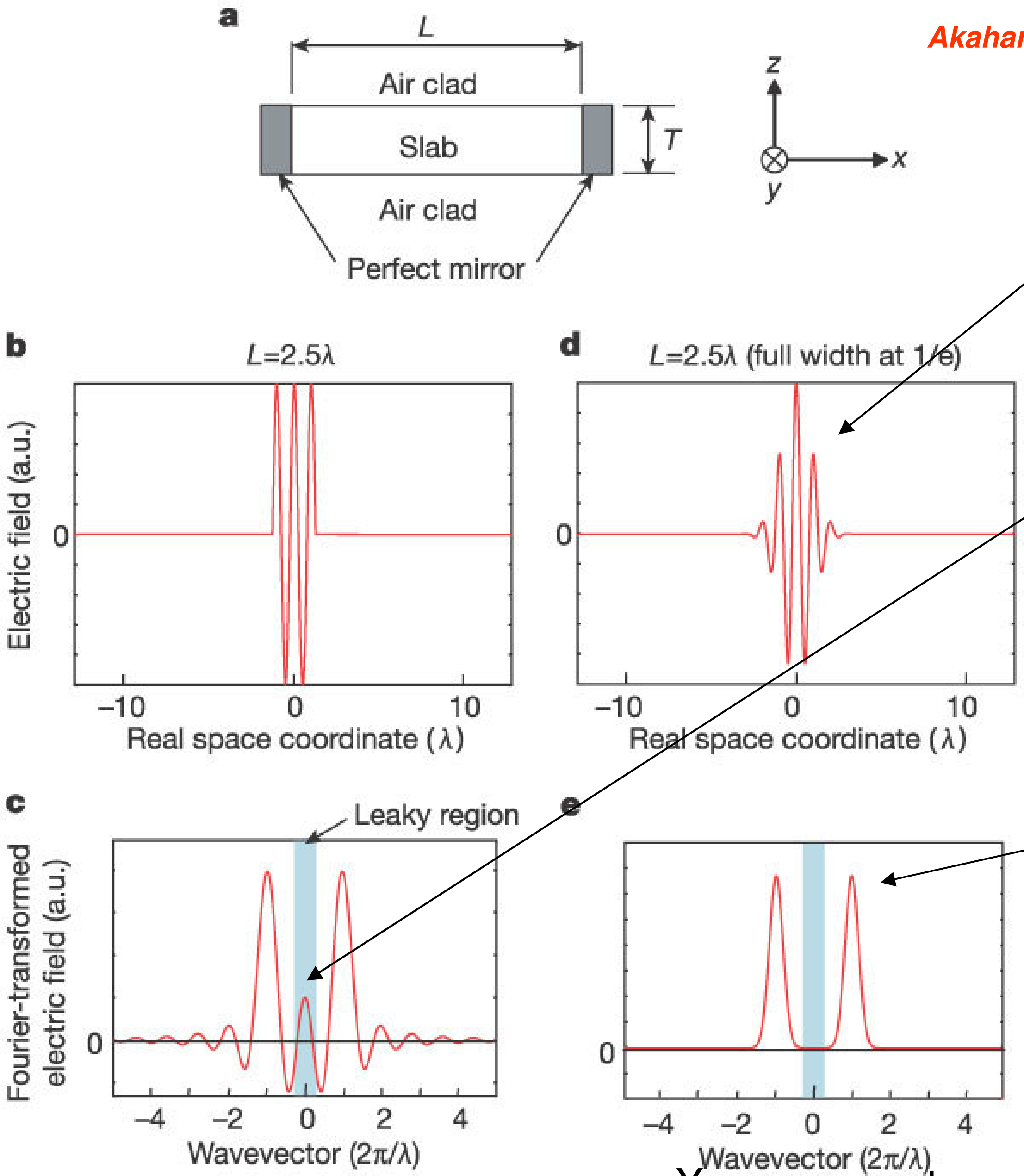

X-component

Gentle Gaussian envelope

In the Leaky region, TIR conditions are not satisfied, light is not confined in the slab

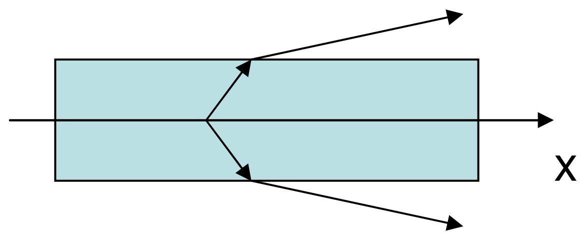

No out of plane leaks.
The cavity modes contains only wavevevector components which fulfill TIR

Room temperature continuous-wave lasing in photonic crystal nanocavity

Masahiro Nomura, Satoshi Iwamoto, Katsuyuki Watanabe, Naoto Kumagai, Yoshiaki Nakata, Satomi Ishida, and Yasuhiko Arakawa

Institute of Industrial Science, Research Center for Advanced Science and Technology, and Nanoelectronics Collaborative Research Center, University of Tokyo, Tokyo 153-8505, Japan
nomura@iis.u-tokyo.ac.jp

Abstract: We demonstrate room temperature continuous-wave laser operation at 1.3 μm in a photonic crystal nanocavity with InAs/GaAs self-assembled quantum dots by optical pumping. By analyzing a coupled rate equation and the experimental light-light characteristic plot, we evaluate the spontaneous emission coupling factor of the laser to be ~ 0.22. Three-dimensional carrier confinement and a low transparent carrier density due to volume effect in a quantum dot system play important roles in the cw laser operation at room temperature as well as a high quality factor photonic crystal nanocavity.

OCIS codes: (250.5230) Photoluminescence; (230.3990) M:

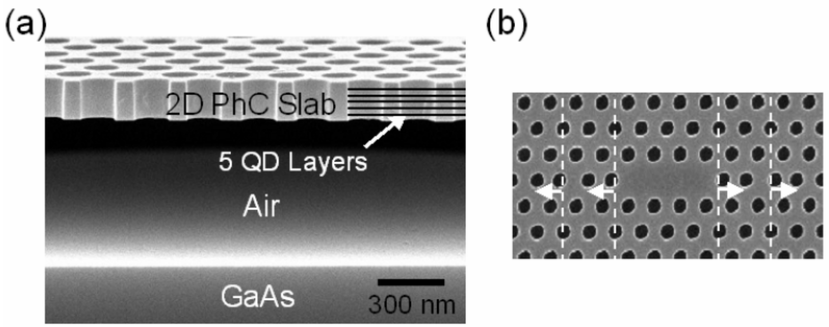

Fig. 1. (a) Scanning electron micrograph of a cross section of a two-dimensional PhC structure. (b) Top view of the L3 defect nanocavity. The first and third nearest air holes at both ends of the cavity are shifted outwards by 0.15*a* as shown by white arrows.

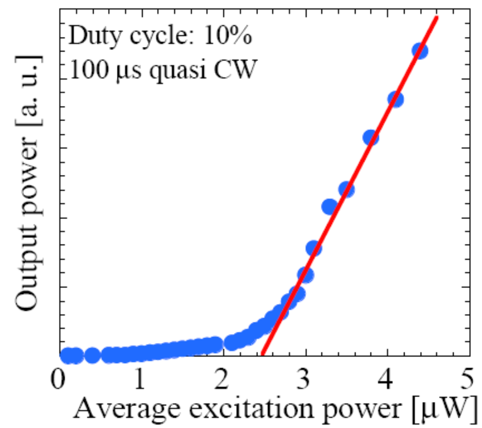

Fig. 3. Output power of the lasing mode as a function of excitation power. The lateral axis is average excitation power (10% duty cycle, 100 μs quasi cw excitation). Red line is the linear fit for the experimental plot above the threshold.

Heterostructure Photonics nanocavity

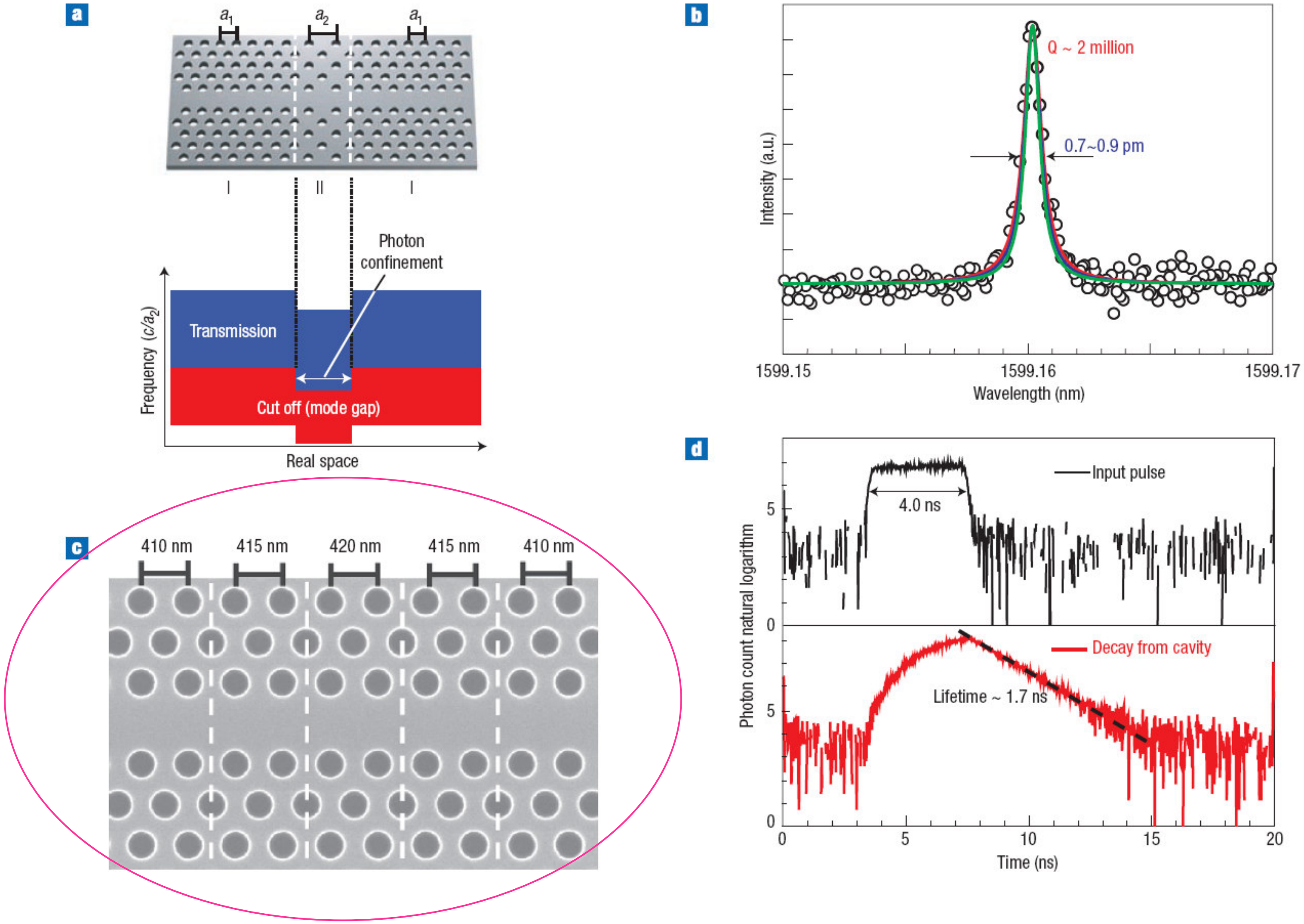

Figure 8 Ultrahigh-*Q* heterostructure photonic nanocavity. **a**, Schematic of heterostructure photonic nanocavity and its light-confinement mechanism[17]. (*c* is the speed of light in a vacuum). Copyright (2005) *Nature Mater.* **b**, Resonant spectrum of a two-step heterostructure nanocavity. An extremely high *Q* factor of 2 million was successfully achieved. **c**, SEM image of the nanocavity used in **b**. Reproduced with permission from ref. 75. Copyright (2006) IEEE. **d**, Time response of the nanocavity where the upper part shows the input pulse to the nanocavity, and the lower part shows the decay from the nanocavity.

Applications of Photonic Crystals for Biosensing

Filters and Detectors:
Interferential filters are multilayer stacks, Ph.C resonat filters can also improve detection.
Efficiency of semiconductor detectors can be maximized (moth's eye patterning)

LASER (source):
Band edge lasers, VCSEL,
High Q cavity for low threshold lasing

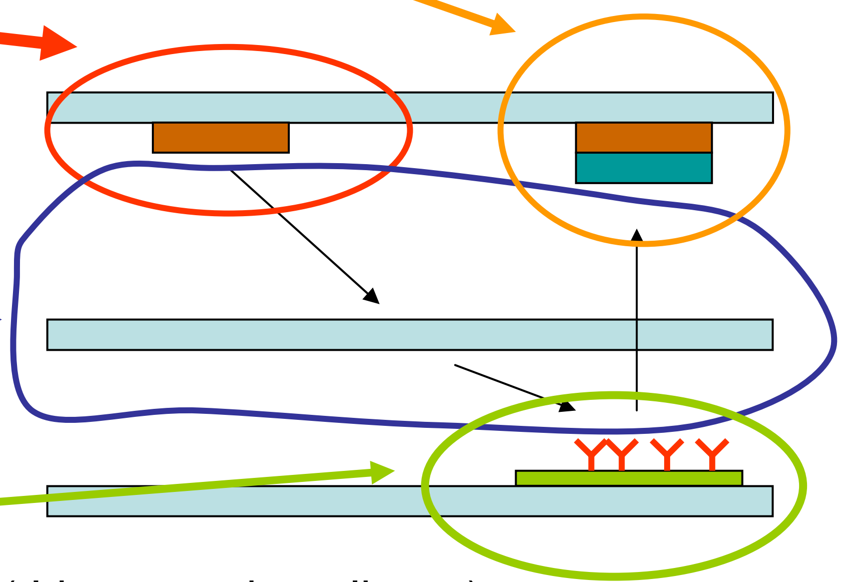

Micro-optics, light manipulation:
Ph.C waveguides, Super prism effect,
wavelength demultiplexer, negative
refraction for perfect micro-lens

Sensor:
Slow light for enhanced light-matter interaction (Linear and nonlinear)
Selective coupling of light can be tuned by infiltration of micro fluids or deposition of bio material on the Ph.C. surface.
Enhanced laser excitation of fluorescent molecules near the Ph.C. surface

Applications of Photonic Crystals for Biosensing

Filters and Detectors
LASER (source)
Micro-optics
Sensor

+ Micro fluidics + Electronics

Using photonic crystals they could be enclosed in a single chip

↓

LAB on a chip

Photonic Crystals Biosensors

Label-free detection: the sensor operates by measuring changes in the wavelength of reflected light as biochemical binding events take place on the surface. For example, when DNA is deposited on the PC surface, an increase in the reflected wavelength occurs only where the mass density of the DNA results.

P. Y. Li, B. Lin, J. Gerstenmaier, B. T. Cunningham
Sensors and Actuators B 99 (2004) 6–13

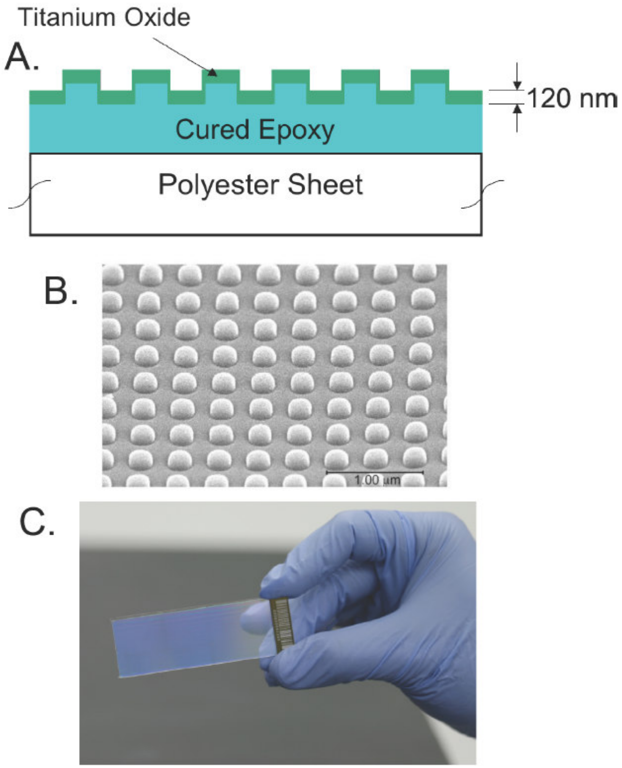

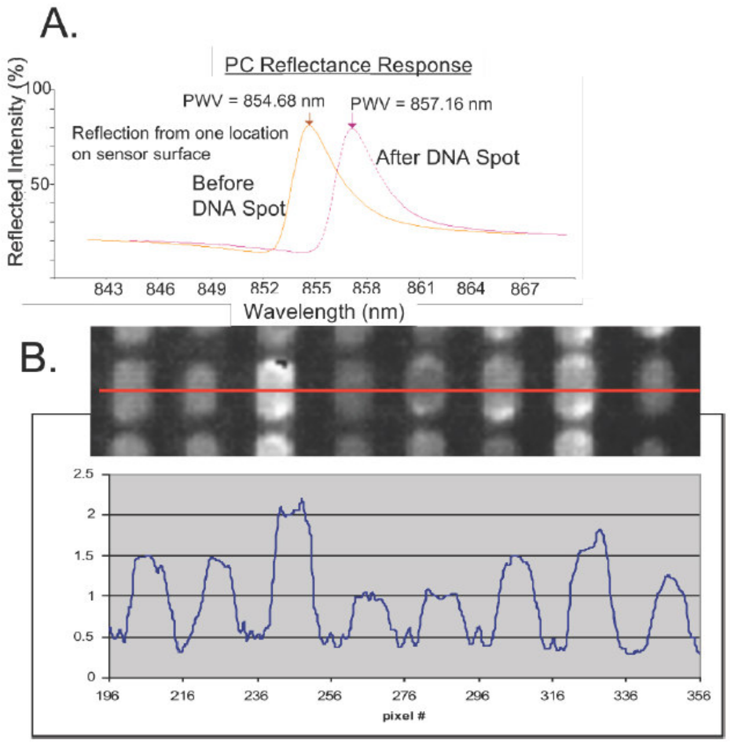

Figure 2. Label-free detection of the adsorption of DNA on the PC surface by quantifying the shift in the resonantly reflected peak wavelength value (PWV). (A) Measurement of ~2.5nm PWV shift due to the attachment of DNA to one location on the PC surface. (B) PWV shift image of a small section from a DNA microarray. Each DNA spot is ~100μm in diameter.

Photonic Crystals Biosensors

The amount of wavelength shift is proportional to the deposited mass density. The readout instrument is able to detect deposited mass changes on the surface with resolution less than 1pg/mm2, and a spatial resolution of 4μm per pixel.

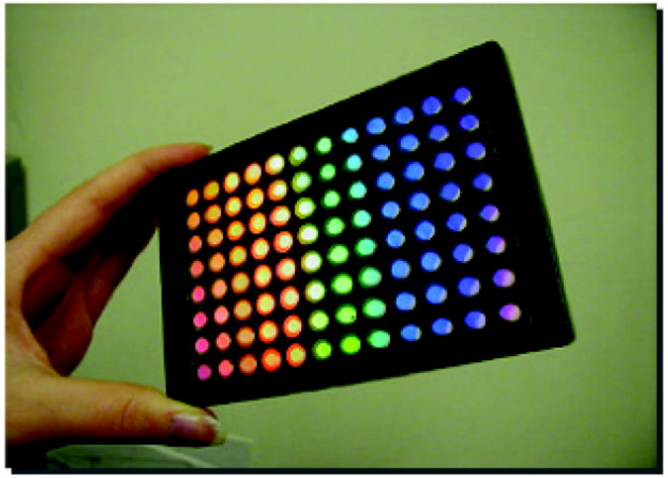

Clean (theory)

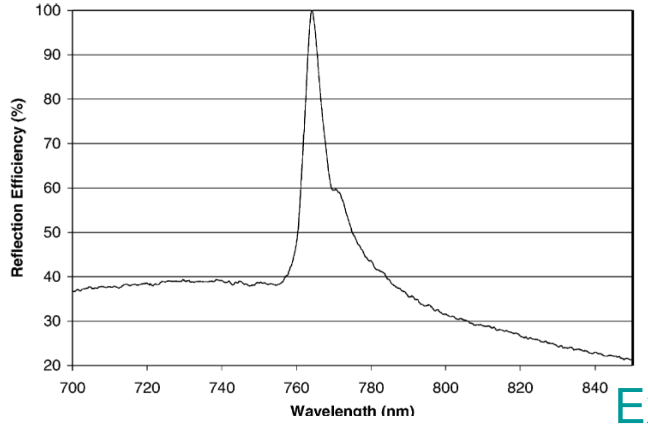

Experiment

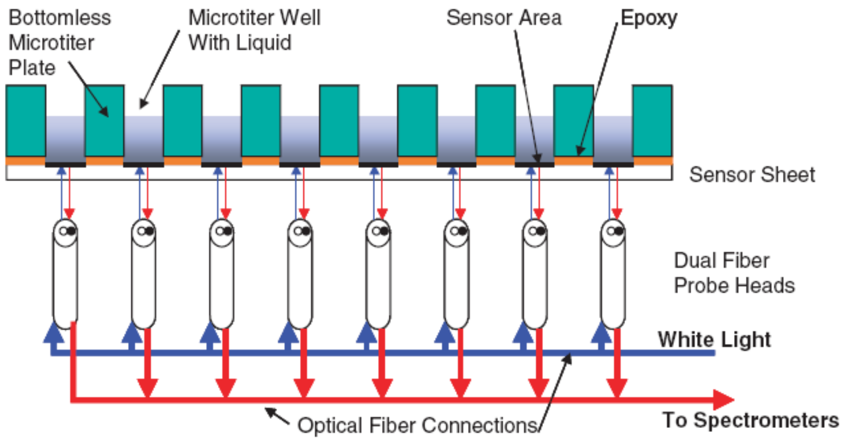

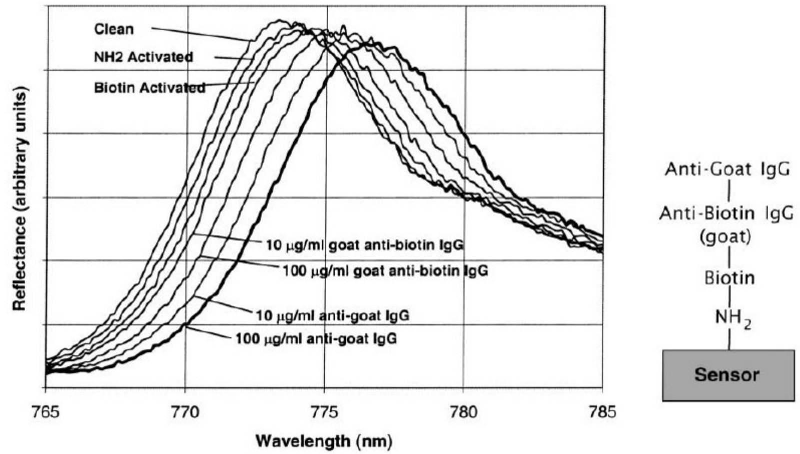

Journal of Biomolecular Screening 9(6); 2004

B. Cunningham et al. / Sensors and Actuators B 81 (2002) 316–328

Photonic Crystals Biosensors

The transmission and reflection spectra of the guided resonance exhibit Fano line shapes. A very important and attractive characteristic of these line shapes is the very sharp variation of the transmission coefficients from 0% to 100% over a narrow frequency range.

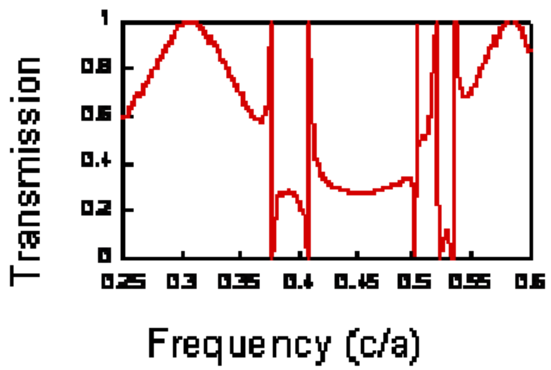

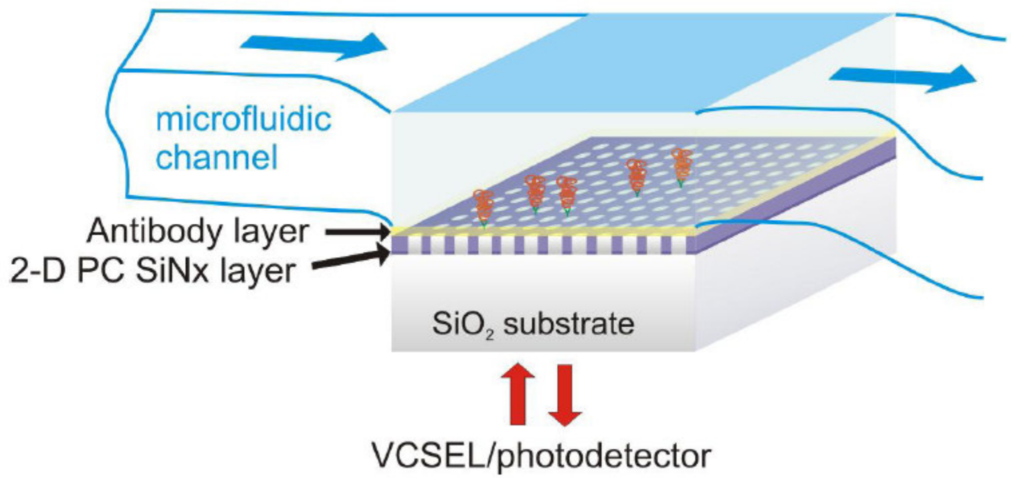

sensor that detects index-of-refraction changes in an aqueous solution utilizing guided resonances. The resonant peak widths and the expected peak shifts were designed with a 0.2 nm spectral line width of a typical VCSEL light source in mind.

A peak shift $\Delta\lambda$=0.2nm corresponds to a detectable index change $\Delta n = 1.5\times10^{-3}$.

O. Levi, Proc. of SPIE Vol. 6447 64470P-9

Photonic Crystals Biosensors

Two-dimensional silicon photonic crystal based biosensing platform for protein detection

Mindy Lee[*] and Philippe M. Fauchet

The Institute of Optics, [2]Department of Electrical and Computer Engineering, University of Rochester
Rochester, New York 14627
[*]mindylee@optics.rochester.edu

Abstract: We theoretically and experimentally demonstrate an ultra-sensitive two-dimensional photonic crystal microcavity biosensor. The device is fabricated on a silicon-on-insulator wafer and operates near its resonance at 1.58 μm. Coating the sensor internal surface with proteins of different sizes produces a different amount of resonance redshift. The present device can detect a molecule monolayer with a total mass as small as 2.5 fg. The device performance is verified by measuring the redshift corresponding to the binding of glutaraldehyde and bovine serum albumin (BSA). The experimental results are in good agreement with theory and with ellipsometric measurements performed on a flat oxidized silicon wafer surface.

OCIS codes: (170.4580) Optical diagnostics for medicine; (230.5750) Resonators

16 April 2007 / Vol. 15, No. 8 / OPTICS EXPRESS 4530

Photonic Crystals Biosensors

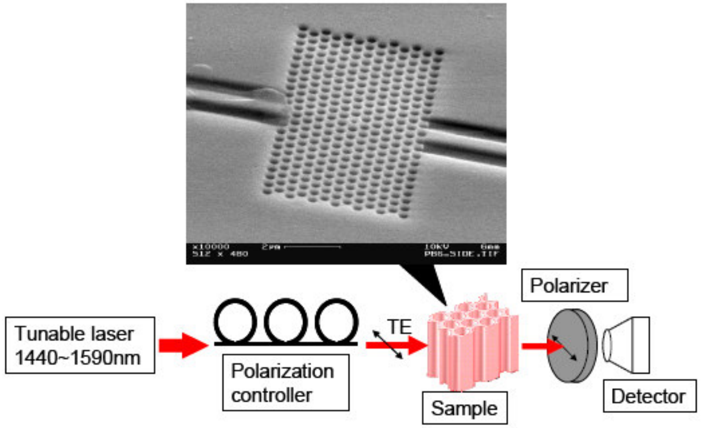

Fig. 1. Scanning electron microscopy photograph of a typical device and schematic of the experimental setup. A tunable laser (1440 nm to 1590 nm) is used as the source. Light is coupled in and out of the PC using tapered ridge waveguides. A polarization controller is used to maximize the TE mode signal, and an InGaAs detector is used to measure the transmission signal.

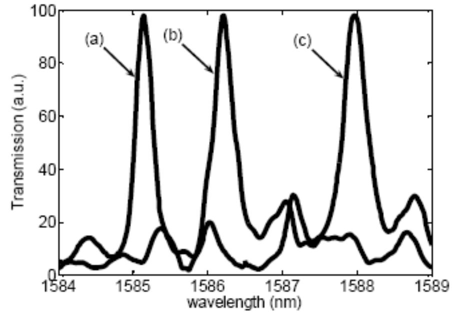

Fig. 3. Normalized transmission spectra of the PC microcavity. Curve (a) indicates the initial spectrum resonance after oxidation and silanization, curve (b) is measured after glutaraldehyde attaches to the pore walls, and curve (c) is obtained after infiltration of BSA molecules.

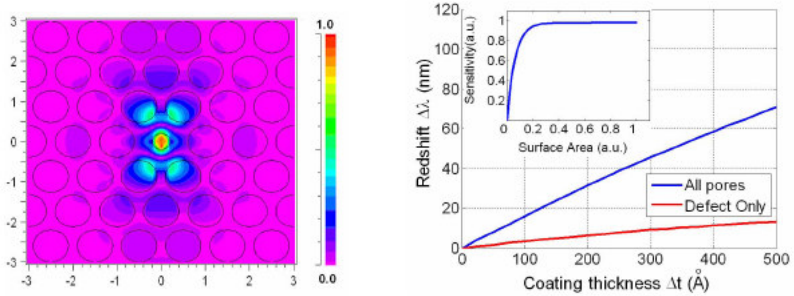

(a) (b)

Fig. 5. (a) Schematic of field confinement in a 2-D PC microcavity (the scales are in μm). The colorbar indicates the scale of electric field intensity. (b) Resonance redshift versus coating thickness on the pore walls. The blue curve shows the redshift due to the uniform infiltration of bio-molecules in all the pores. The red curve shows the redshift due to the infiltration only in the central defect. The inset at the top left shows the normalized sensitivity (Δλ/Δt) vs. the surface area covered by the bio-molecules. If the region coated with bio-molecules extends to pores away from the defect, the sensitivity first increases rapidly and then saturates.

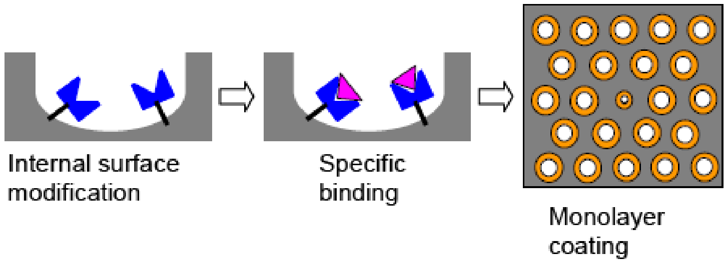

(a) (b)

Fig. 2. Schematic of bio-molecule recognition: (a) the target molecules are captured by the probe molecules. (b) The bio-molecules form a uniform layer on the internal surface of the sensor. In reality the layer thickness is very small compared with the pore size.

Photonic Crystals Biosensors

Fluorescence biodetection: the 2D PC period can be selected to provide a resonance for enhancing the laser excitation of fluorescent molecules near the PC surface. Since the excited leaky modes are radiative but localized in space during their finite lifetimes, they can be engineered to have very high energy density within regions of the PC at resonance. The intensity of emission of fluorescent samples that are absorptive at the resonant wavelengths can thus be greatly enhanced by placing them in proximity to regions where the resonant modes concentrate most of their energy. Also extraction of emitted fluorescence can be maximized.

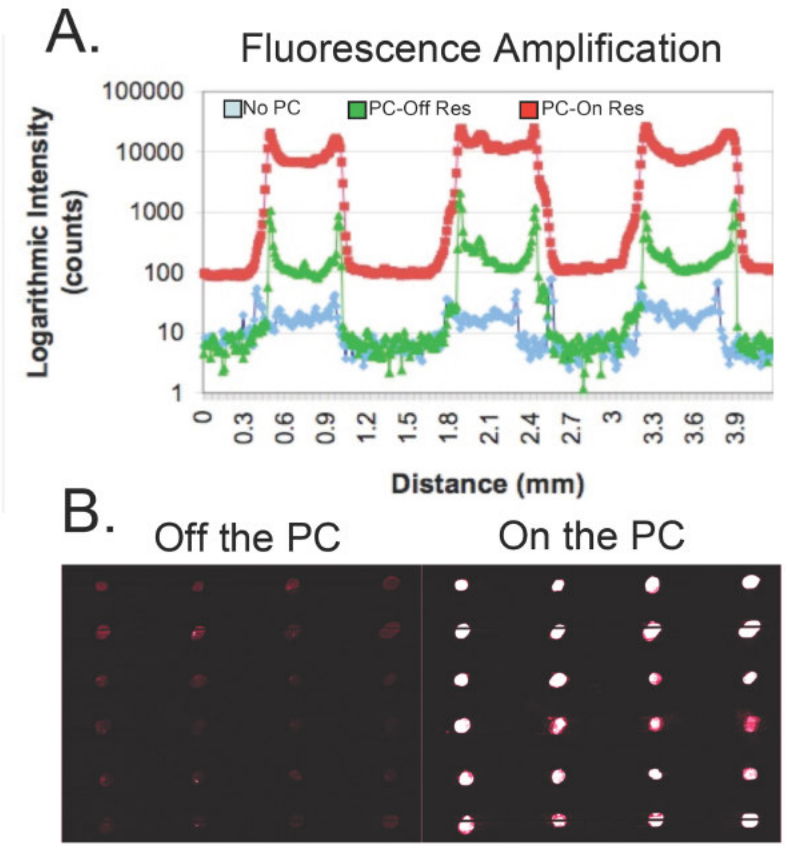

(A) Cross-section intensity images of 500µm-diameter spots of streptavidin-Cy5 compared without a PC, on the PC illuminated at an off-resonant angle, and on the PC measured at resonance: a $535\times$ gain is demonstrated compared to the No-PC case. (B) Images of fluorescence intensity from 500µm-diameter spots of streptavidin-Cy5 on an unpatterned TiO_2 surface and an adjacent photonic crystal region on the same surface when the incident laser light matches the resonant condition.

P. C. Mathias et al. Appl. Opt. 26, pp. 2351–2360, 2007.

Applications of Photonic Crystals for Biosensing

Filters and Detectors:
Interferential filters are multilayer stacks, Ph.C resonat filters can also improve detection.
Efficiency of semiconductor detectors can be maximized (moth’s eye patterning)

LASER (source):
Band edge lasers, VCSEL,
High Q cavity for low threshold lasing

Micro-optics, light manipulation:
Ph.C waveguides, Super prism effect,
wavelength demultiplexer, negative
refraction for perfect micro-lens

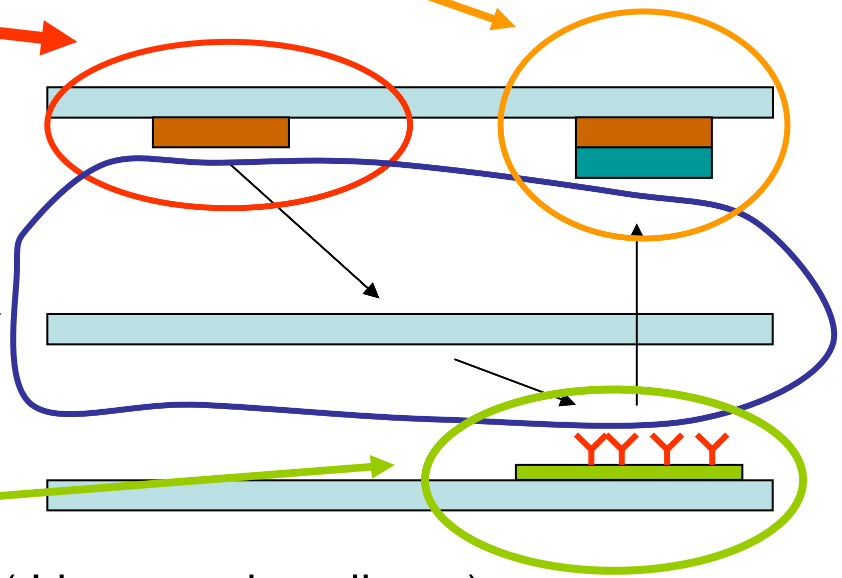

Sensor:
Slow light for enhanced light-matter interaction (Linear and nonlinear)
Selective coupling of light can be tuned by infiltration of micro fluids or deposition of bio
material on the Ph.C. surface.
Enhanced laser excitation of fluorescent molecules near the Ph.C. surface

Compact wavelength demultiplexing using focusing negative index photonic crystal superprisms

Babak Momeni, Jiandong Huang, Mohammad Soltani, Murtaza Askari, Saeed Mohammadi, Mohammad Rakhshandehroo and Ali Adibi

School of Electrical and Computer Engineering, Georgia Institute of Technology, Atlanta, GA 30332 USA
momeni@ece.gatech.edu, jdhuang@ece.gatech.edu, soltani@ece.gatech.edu, murtaza@ece.gatech.edu, saeedm@ece.gatech.edu, adibi@ece.gatech.edu

Abstract: Here, we demonstrate a compact photonic crystal wavelength demultiplexing device based on a diffraction compensation scheme with two orders of magnitude performance improvement over the conventional superprism structures reported to date. We show that the main problems of the conventional superprism-based wavelength demultiplexing devices can be overcome by combining the superprism effect with two other main properties of photonic crystals, i.e., negative diffraction and negative refraction. Here, a 4-channel optical demultiplexer with a channel spacing of 8 nm and cross-talk level of better than -6.5 dB is experimentally demonstrated using a 4500 μm^2 photonic crystal region.

OCIS codes: (999.9999) Photonic crystals; (999.9999) Superprism; (130.3120) Integrated optics devices

Ph.C. based Wavelength demultiplexer in a Silicon-on-insulator (SOI) substrate. Before entering into the PC region, the incident optical beam (with multiple channels) propagates in the unppatterned Si. (broadeining of the beam (preconditioning)

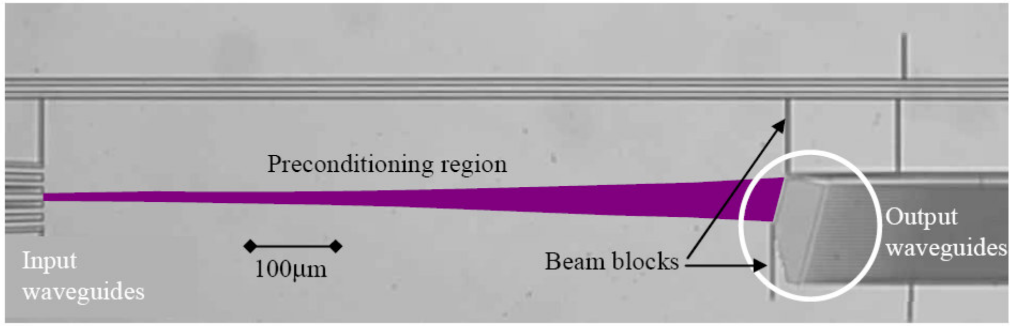

As the beams propagate through the Ph. C. , they expereince 3 basic effects: Superprism effect, negative diffraction and negative refraction

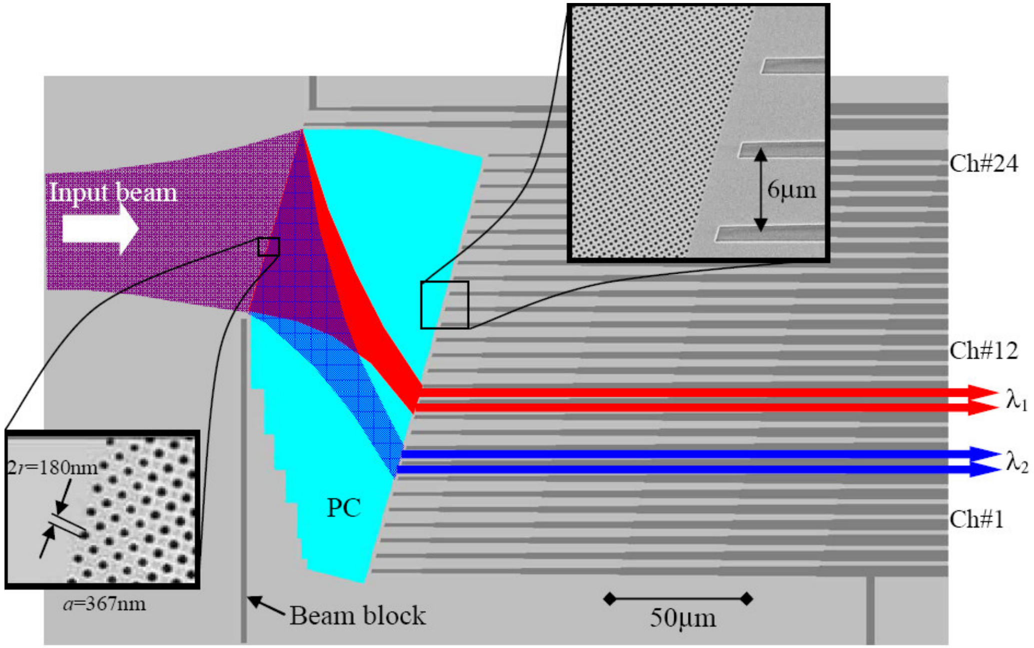

Beams of different wavelengths propagate in different directions inside the PC (Superprism), plus difraction is compensated at the output

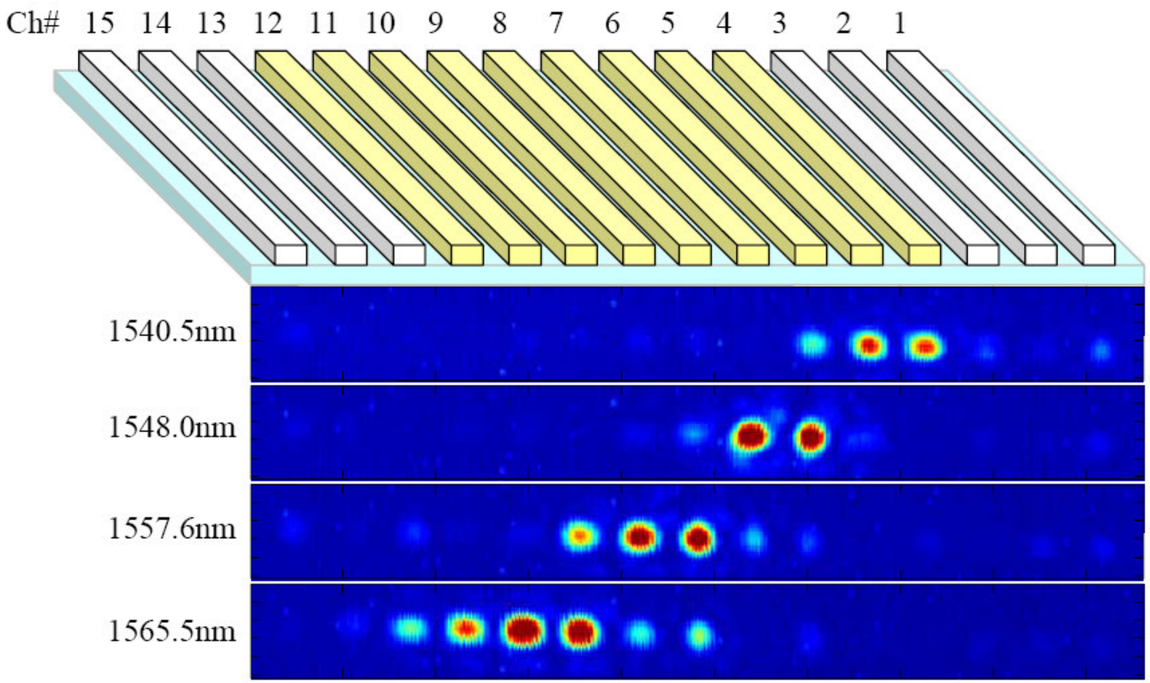

Photonic Crystal Fibers

Guiding light: Conventional Optical Fibres

- Total Internal Reflection (TIR)
  - $n_{Cladding} < n_{Core}$
  - Core must be dielectric material
  - Interaction between light and matter unavoidable
    - Non-linearity
    - Material Dispersion
    - Losses

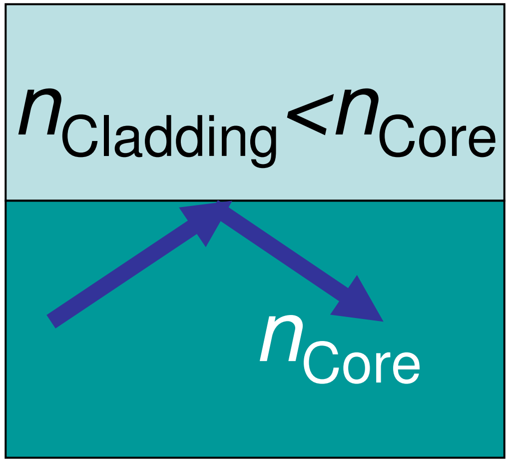

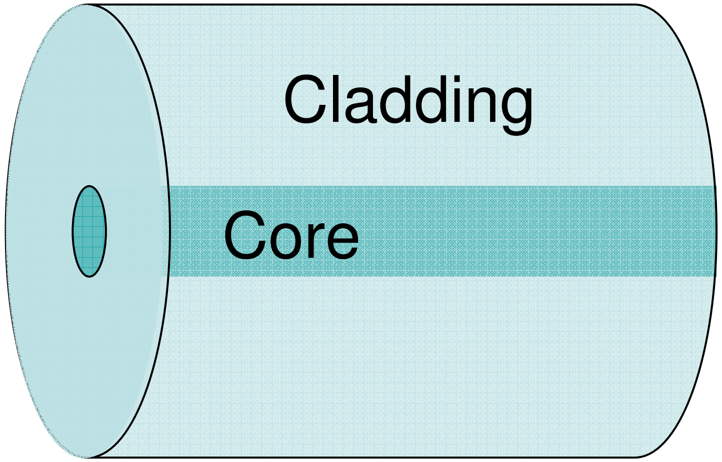

$n_{Core} > n_{Cladding}$

http://www.physics.usyd.edu.au/cudos/

Photonic Crystal Fibers

- Bragg reflection
  - Very low losses
  - Bandwidth ?
  - Angle of incidence ?
  - Index contrast ?
  - Fabrication ?

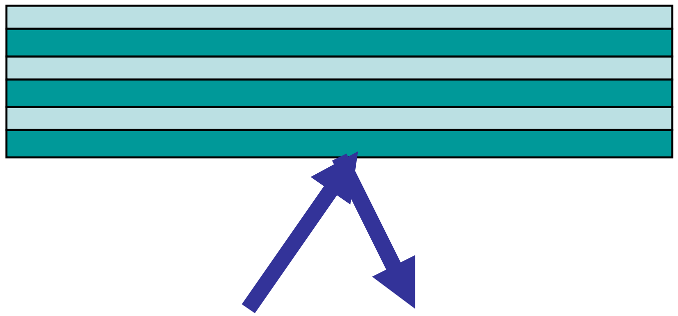

- Bragg fibres, “OmniGuide” fibres

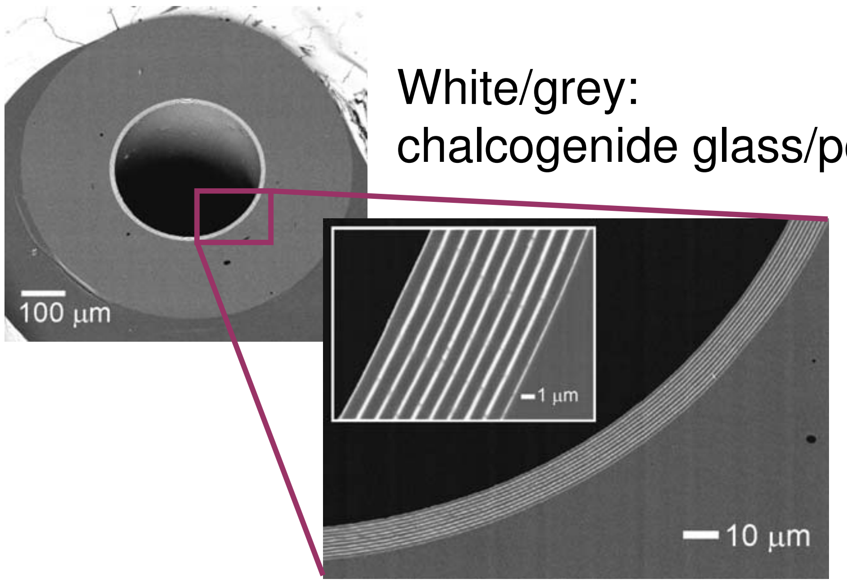

White/grey:
chalcogenide glass/polymer

Burak Temelkuran *et al*
Nature <u>420</u>, 650-653, December 2002.

Photonic Crystal Fibers

Applications of Omniguide fibers

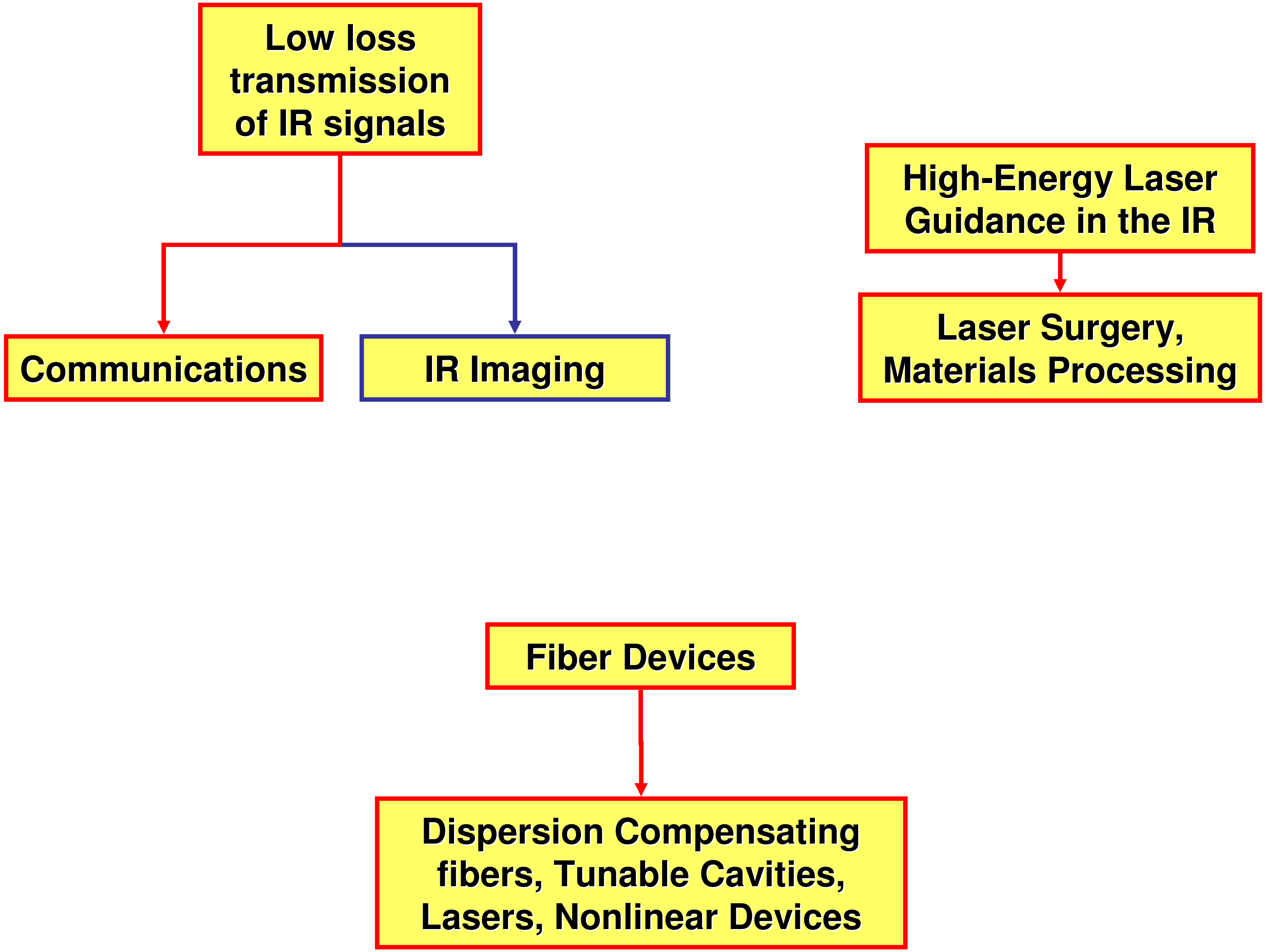

High-Power Transmission

at 10.6µm

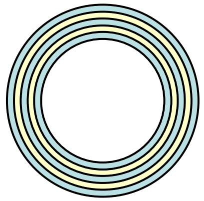

Polymer losses @10.6µm ~ 50,000dB/m…

…waveguide losses < 1dB/m

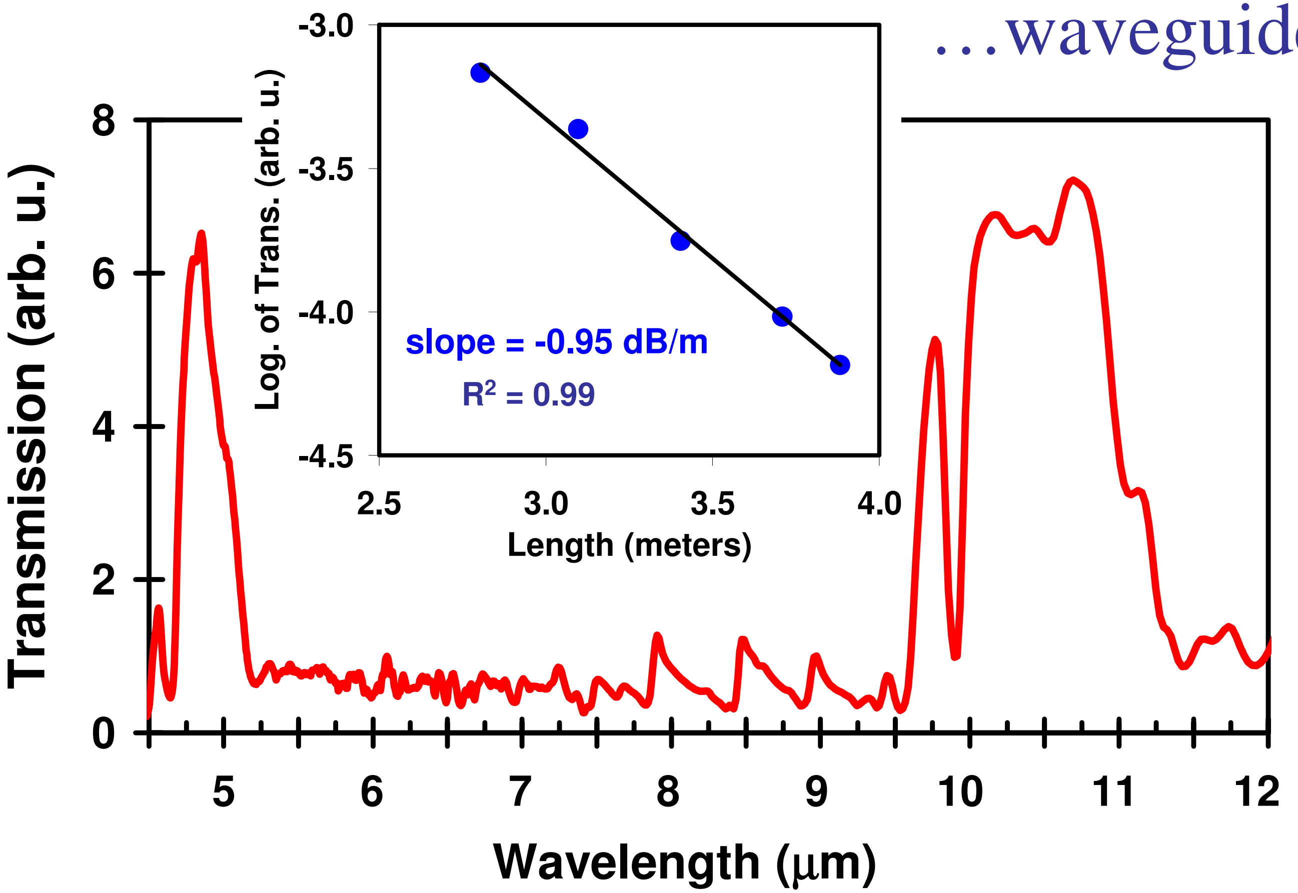

[B. Temelkuran *et al.*, *Nature* **420**, 650 (2002)]

[Y. Fink *et al.*, MIT]

High-Power Transmission

at 10.6μm

*CO_2 lasers have been used for years to treat patients diagnosed with Recurrent Respiratory Papillomatosis **RRP**.*
RRP involves tumor growths in the larynx and trachea that can lead to total obstruction of the breathing passages and ultimate death.

In the past, a CO_2 laser ablation procedure could only be performed in the operating room, with patient under general anesthesia, because of the need to dislocate the jaw, in order to bring in the laser.

*On November 19, 2004, a critically ill patient suffering from severe RRP (who could not undergo general anesthesia) was operated on by **Dr. Jamie Koufman**, Wake Forest Hosptial, NC using an OmniGuide CO_2 laser fiber, in the first such minimally–invasive procedure. The patient was awake during the procedure and required only a topical anesthetic.*

http://ab-initio.mit.edu/mpb

Photonic Crystal Fibers

Birks, Roberts, Russel, Atkin, Shepherd, Electron.
Lett. **31**, 1941-1942 (1995)

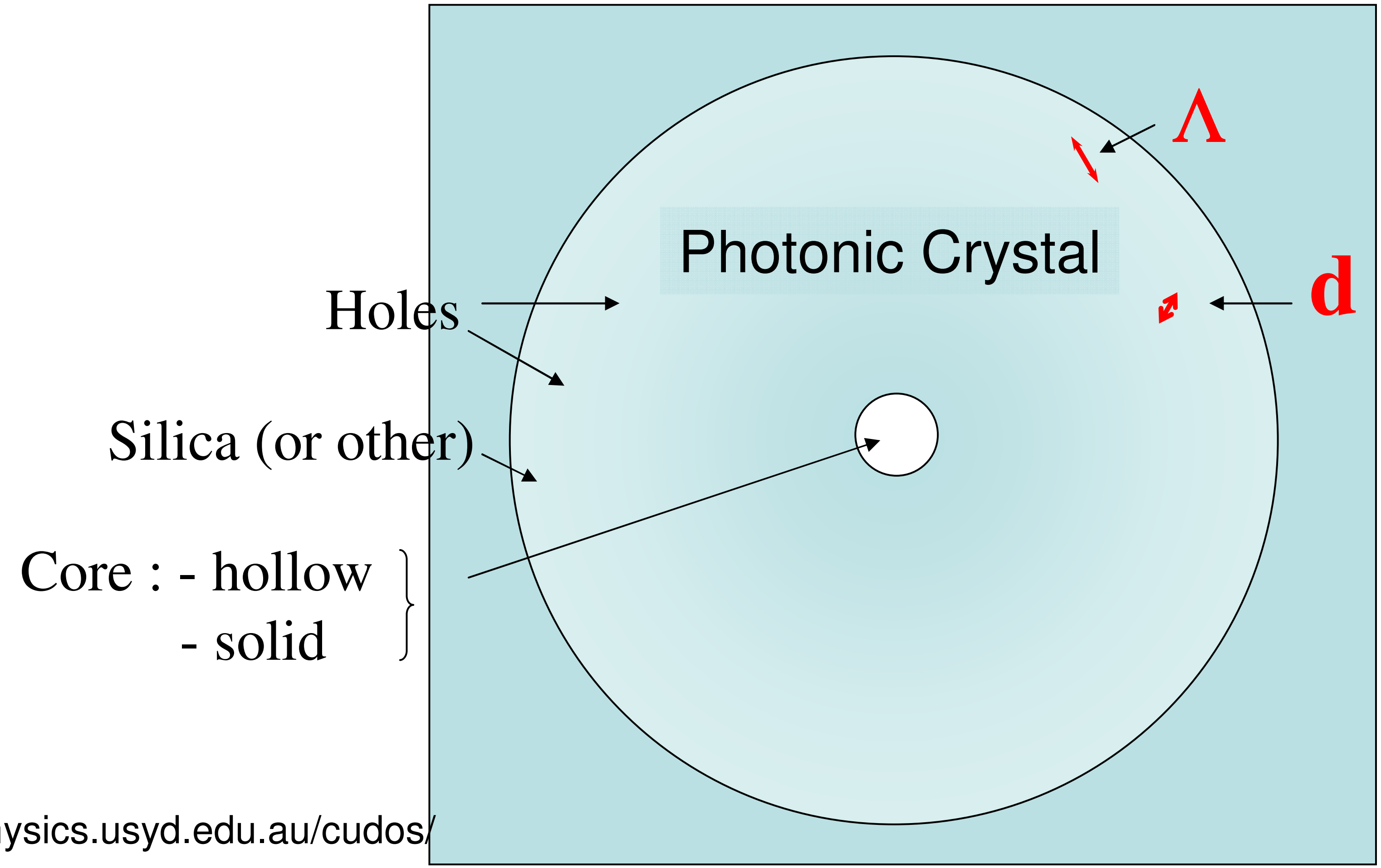

http://www.physics.usyd.edu.au/cudos/

Photonic Crystal Fibers

Holey Silica Cladding

- Hollow core and solid core PCFs

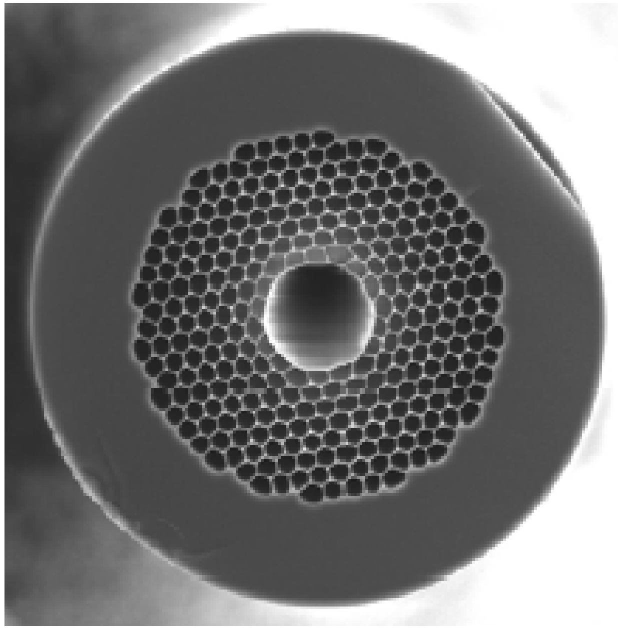

Mangan *et al*, OFC 2004
(1.7dB/km Loss@1550nm)

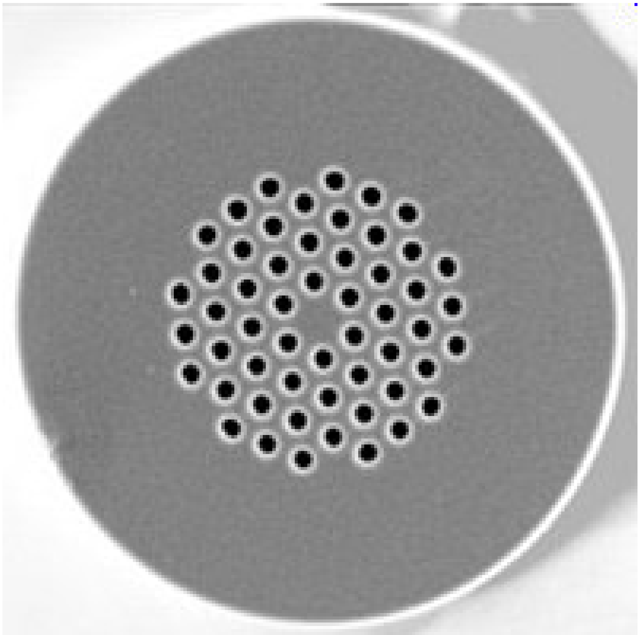

blazephotonics

Photonic Crystal Fibers

Hollow Core and Holey Silica Cladding

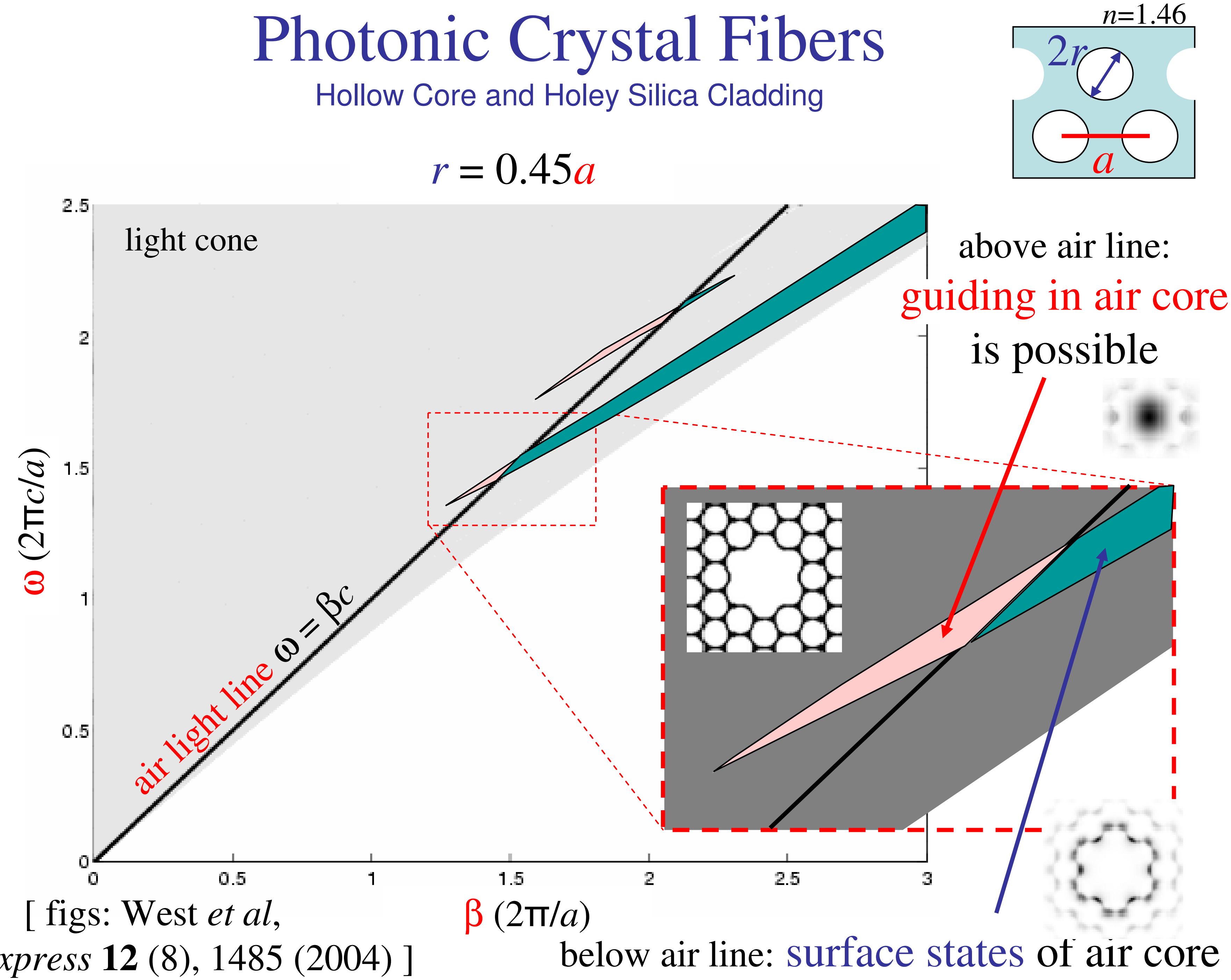

[figs: West *et al*, *Opt. Express* **12** (8), 1485 (2004)]

Photonic Crystal Fibers

Effective index vs PBG guidance

Mechanism	TIR "averaged index"	coherent scattering
Periodicity	Not necessary	Crucial
Bandwidth	Unlimited	$\Delta\lambda/\lambda \sim 10\%$
Core	Solid	Hollow or solid
Hole/pitch	Small or large	Large (typ. $d/\Lambda > 0.9$

Photonic Crystal Fibers

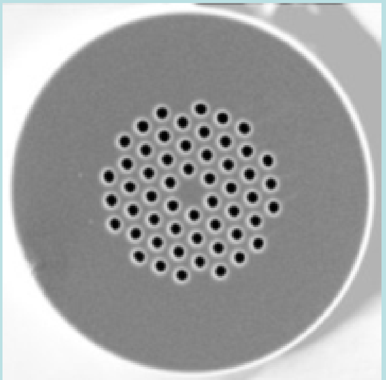

Blaze Photonics

Solid core: Striking Properties

- "Endlessly single-mode"
- Large effective area
- *or* Tight confinement
- Highly adjustable dispersion
- Adjustable birefringence

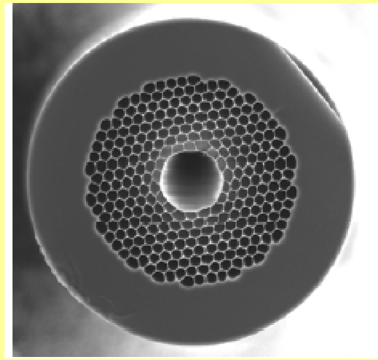

Mangan *et al*, OFC 2004

Hollow core (Bragg&PCF): Properties

- >97% light in air, <3% in silica
- Highly reduced
  - Non-linearity
  - Material absorption
  - Material dispersion
- Bandwidth: $\Delta\lambda/\lambda \sim 10\%$
- Large Waveguide dispersion
- Typically "multimode"

Photonic Crystal Fibers

Hollow core

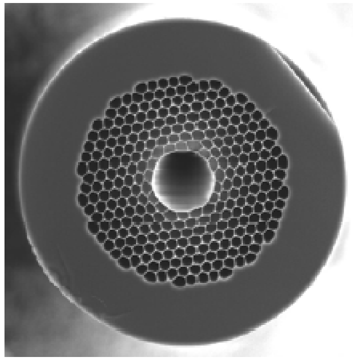

- Applications
  - High power delivery
  - Non-conventional wavelengths
  - High power pulse compression
  - Telecom
  - Gas based non-linear optics
    - Raman; high-order harmonic generation…
  - Particle guidance
  - Sensing

Photonic Crystal Fibers

solid core

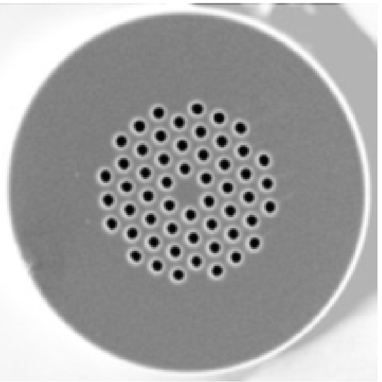

Blaze Photonics

“Endlessly” single-mode

[T.A. Birks et al Opt. Lett. **22**, pp. 961-963 (1997)]

If $d/\Lambda<0.406$ the fundamental mode is the only mode guided in the core, regardless of wavelength !

Single-mode fibres with arbitrarily large cores$\rightarrow$ for same power reduced NL

High power fibre-amplifiers
High power fibre-lasers

Photonic Crystal Fibers

solid core

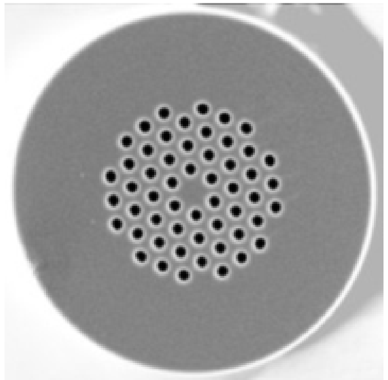

Blaze Photonics

Single-mode fibre with small core

Single-mode broad spectrum…
Tight confinement
Enhancement of NL effects

Combination of ultra-high NL, adjustable dispersion:

Solitons in the visible

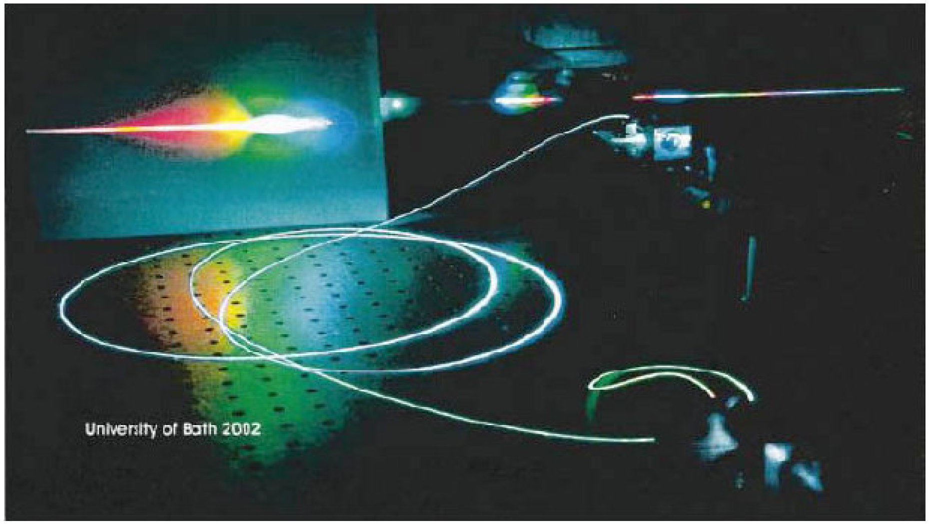

"Super-continuum" generation

output characteristics

390-1600nm flat spectrum
Coherent, Single-mode

Photonic Crystal Fibers

- Further reading:
- Review papers
  - J. C. Knight, “Photonic Crystal Fibres,” *Nature* **424**, pp.847-851 (2003)
  - Ph. Russel, “Photonic Crystal Fibers,” *Science* **299,** pp. 358-362 (2003)
  - B. J. Eggleton, “Microstructured optical Fiber devices,” *Opt. Express* **9**, pp. 698-713 (2001)
  - Optics Express (in general, contains several MOF papers in each issue)
- Books
  - A. Bjarklev *et al*, *Photonic Crystal Fibres*, Kluwer Academic Publishers (2003)
  - F. Zolla *et al, Foundations of Photonic Crystal Fibres,* Imperial College Press (in press).
  - PJ Russel, *Photonic Crystal Fibre*, John Wiley and Sons (2005)

PBG nonlinear enhancement

- Band edge field enhancement: lower the input intensity or reduce the structure size, Improves the efficiency of nonlinear processes and sensitivity to local field effects. Enhanced parametric processes, gap and Bragg solitons.

- Dispersion and diffraction controlled by design: slow light, waveguiding, superprism effects, Phase matching

- Combination of nonlinear and dispersive effects: Gap and Bragg solitons, modulation instabilities.

Second Harmonic Generation in PhC

-P.M. (equal PHASE velocity), **$\Delta k = k_{2\omega} - 2k_{\omega} = 0$**

If such condition is fulfilled, the FF and SH fields propagate with the same phase velocities

It is possible in PhC thanks to the geometrical dispersion and periodicity

$$\boxed{\vec{k}_{Bloch}(2\omega) - 2\vec{k}_{Bloch}(\omega) - \vec{G} = \vec{0}}$$

Where **G** is a reciprocal lattice vector.

-Field enhancement due to *field localization*

(band edge and when T=1)

- Enhanced conversion efficiency

Band Edge Effects

Finite size 1D photonic crystals transmission bands exhibit resonance peaks due to the boundary conditions with the external (homogenous) world.
In particular, resonances are sharper in proximity of the band edge.

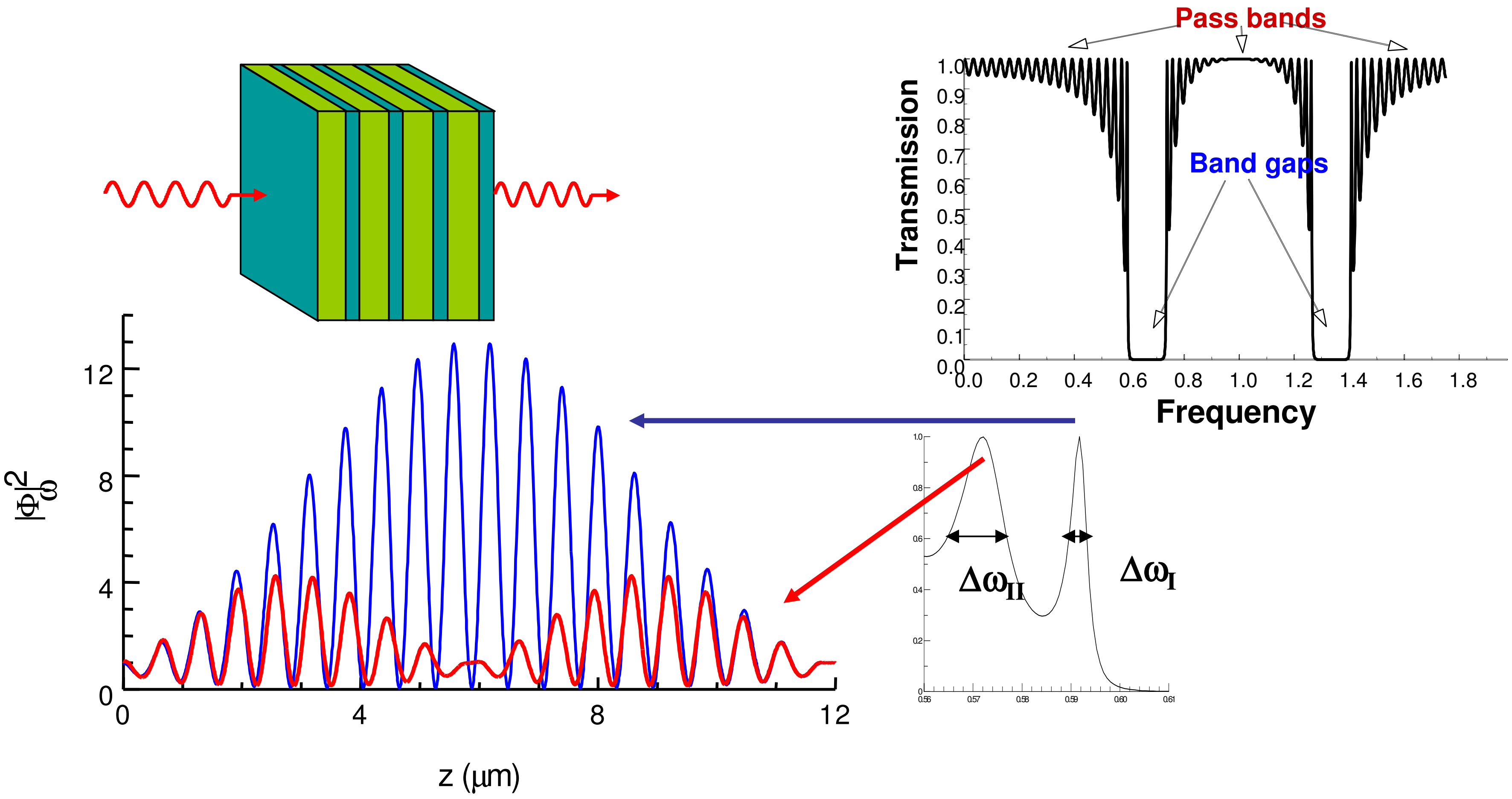

Phase Matching

Effective refractive index

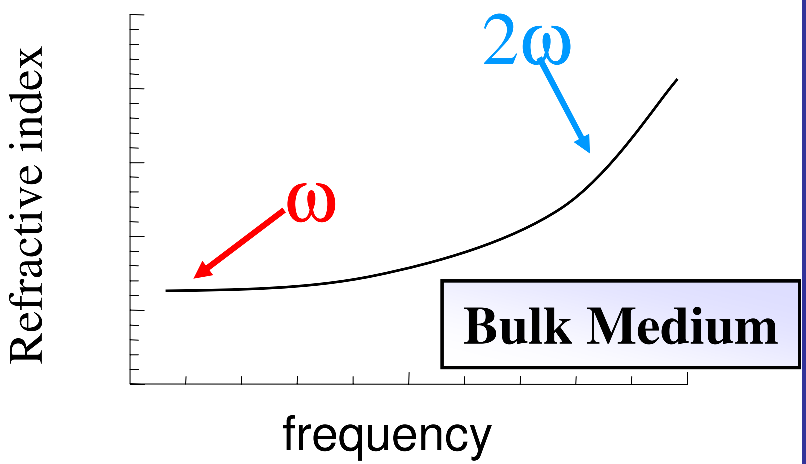

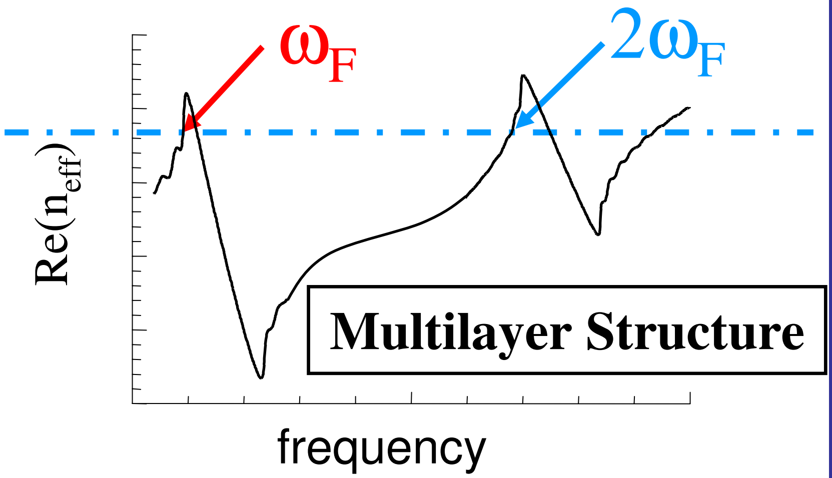

$$t = x + iy \equiv \sqrt{T}\, e^{i\varphi_t} \equiv e^{i\Phi}$$

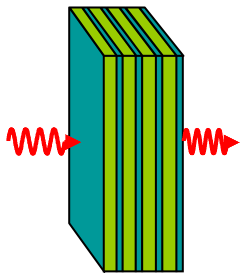

$$\varphi_t = tg^{-1}\left(\frac{y}{x}\right) \pm m\pi$$

$$\Phi = \varphi_t - i \ln\sqrt{T} \equiv \hat{k}_{eff} D \equiv \frac{\omega}{c}\hat{n}_{eff} D$$

$$\hat{n}_{eff} = \frac{c}{\omega D}\left[\varphi_t - \frac{i}{2}\ln(x^2 + y^2)\right]$$

*Centini et al, Phys. Rev. E 60, 4891-4898 (1999)

Does not require periodicity, can be used for every kind of stack

Conversion Efficiency

The expression of the conversion efficiency ($\eta = I_{SH} / I_{pump}$)
in the non-depleted pump regime is similar to the bulk case

$$\eta^{(+,-)} = \frac{8\pi^2 \left| d_{eff}^{(+,-)} \right|^2 L^2 I_{pump}}{\varepsilon_0 c \lambda^2 n_{eff}^{(\omega,p)} n_{eff}^{(\omega,s)} n_{eff}^{(2\omega,p)}}$$

$$\tilde{d}_{eff}^{(+,-)} = \frac{1}{L} \int_0^D \chi^{(2)}(z) \Phi_{\omega}^{2(+)}(z) \Phi_{2\omega}^{*(+,-)}(z) dz$$

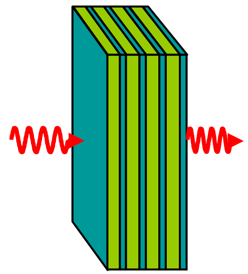

d_{eff} contains both information on PM conditions and fields overlap

*G. D'Aguanno, et al. J. Opt. Soc. Am. B 19, 2111 (2002)

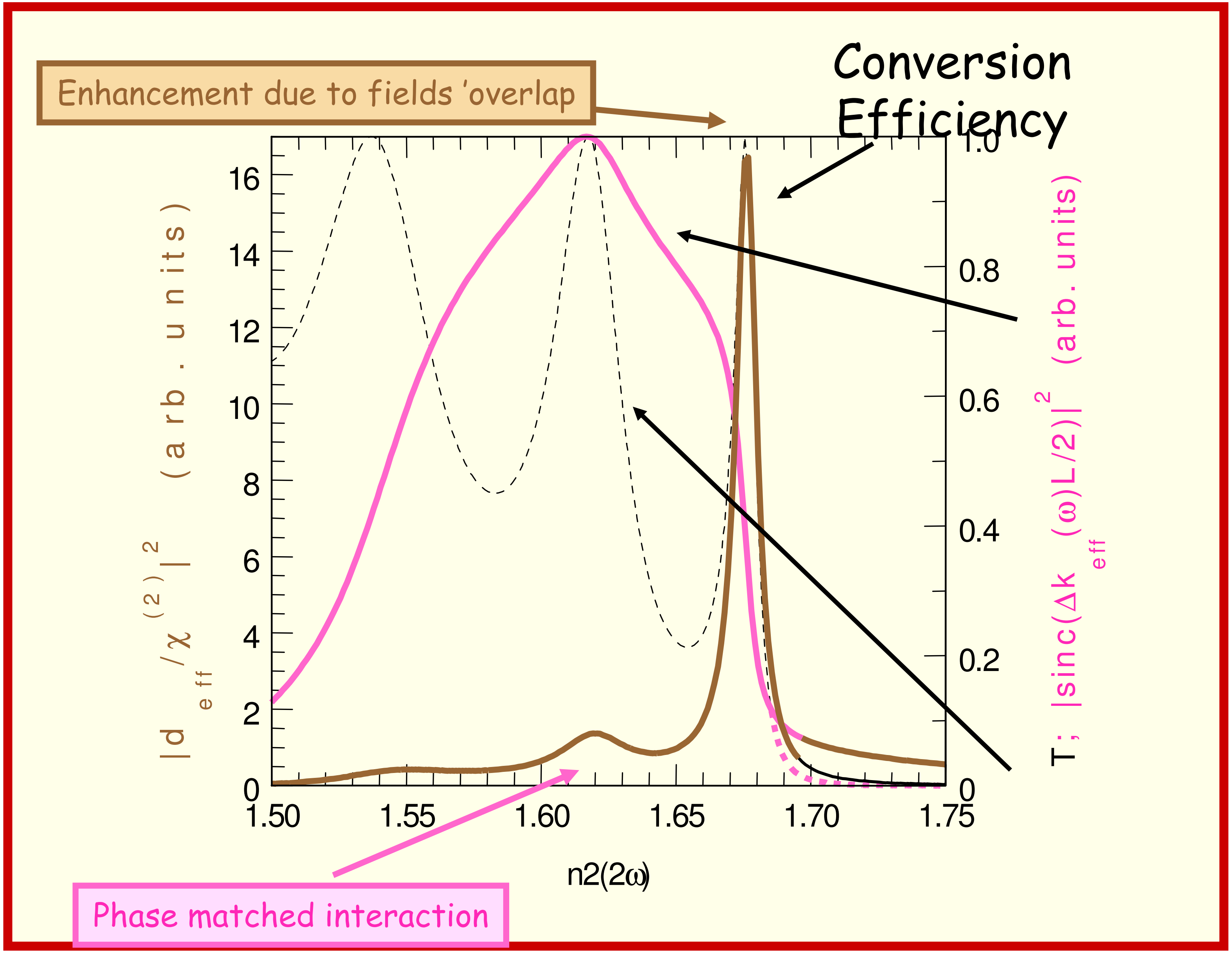

M. Centini et al., Opt. Lett. 29, 1924 (2004)

Non collinear Type II second harmonic generation

APPLIED PHYSICS LETTERS VOLUME 84, NUMBER 16 19 APRIL 2004

Noncollinear type-II second-harmonic generation in a $Al_{(0.3)}Ga_{(0.7)}As/Al_2O_3$ one-dimensional photonic crystal

A. Bosco, M. Centini, L. Sciscione, C. Sibilia,[a] E. Fazio, and M. Bertolotti
Istituto Nazionale di Fisica della Materia, INFM, at Dipartimento di Energetica—Università di Roma "La Sapienza," Via A. Scarpa 16, I-00161 Roma, Italy

A. Fiore
Institute of Quantum Electronics and Photonics—Ecole Polytechnique Fédérale de Lausanne, CH-1015 Lausanne, Switzerland and Institute of Photonics and Nanotechnology, CNR, via del Cineto Romano 42, 00156 Roma, Italy

A. Convertino and L. Cerri
Istituto per lo Studio dei Materiali Nanostrutturati, CNR, via Salaria Km. 29.300, 00016 Roma, Italy

M. Scalora
Weapons Sciences Directorate, AMSRDI-RD-WS-ST, RD&EC, U.S. Army Missile Command, Building 7804, Redstone Arsenal, Alabama 35898-5000

(Received 27 October 2003; accepted 26 February 2004)

We demonstrate noncollinear type-II second-harmonic generation in one-dimensional photonic crystals. A 15-period $Al_{(0.3)}Ga_{(0.7)}As/Al_2O_3$ structure, 3.5 μm long, was designed, fabricated, and experimentally characterized. We measured an effective nonlinearity of (52 ± 12) pm/V in perfect phase-matching conditions. [DOI: 10.1063/1.1713039]

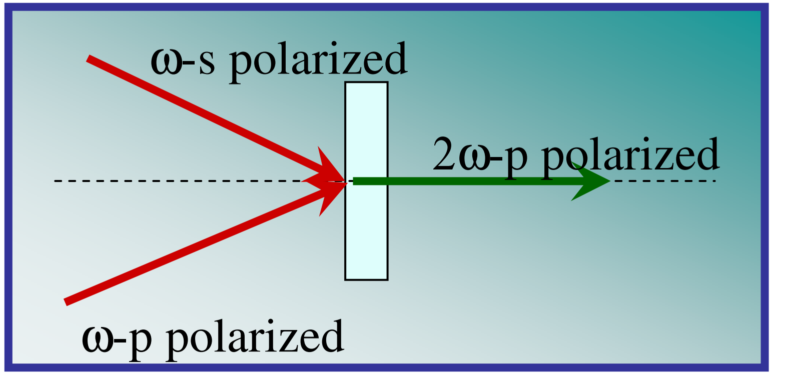

Non collinear Type II second harmonic generation

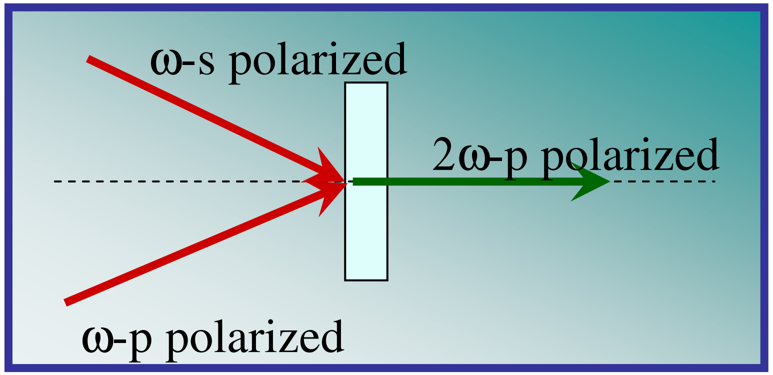

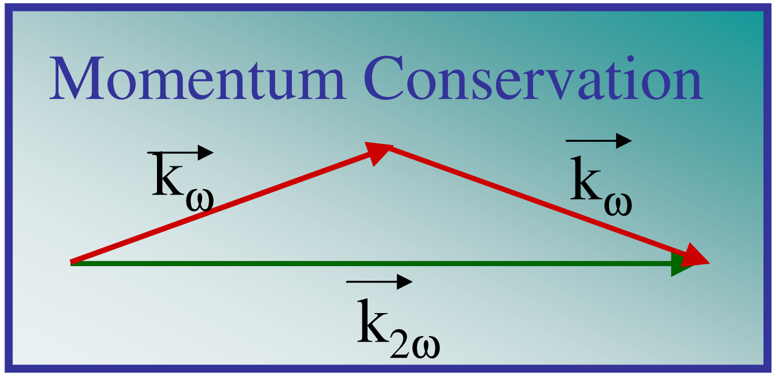

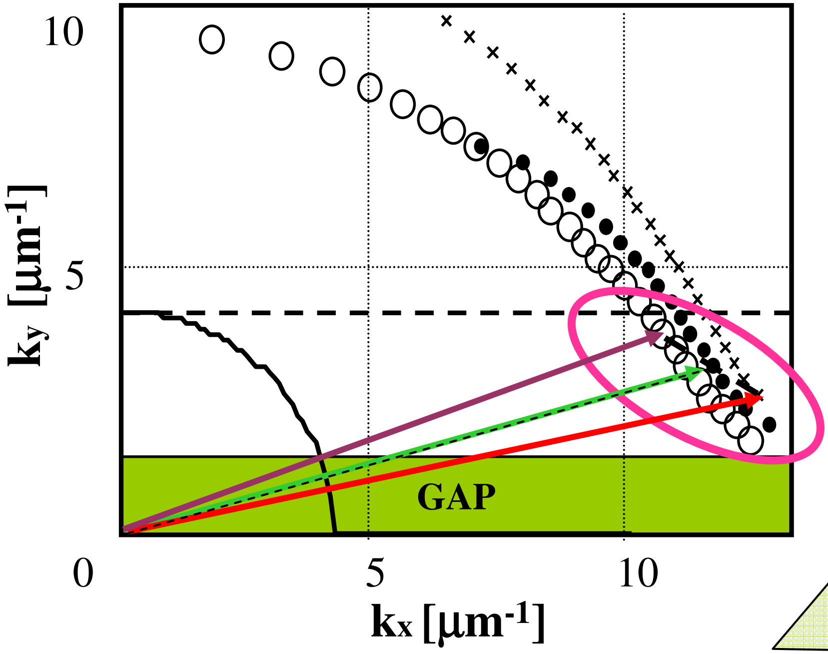

$$\frac{1}{2}\left[\vec{k}^{(\omega,s)}+\vec{k}^{(\omega,p)}\right]=\frac{1}{2}\vec{k}^{(2\omega,p)}$$

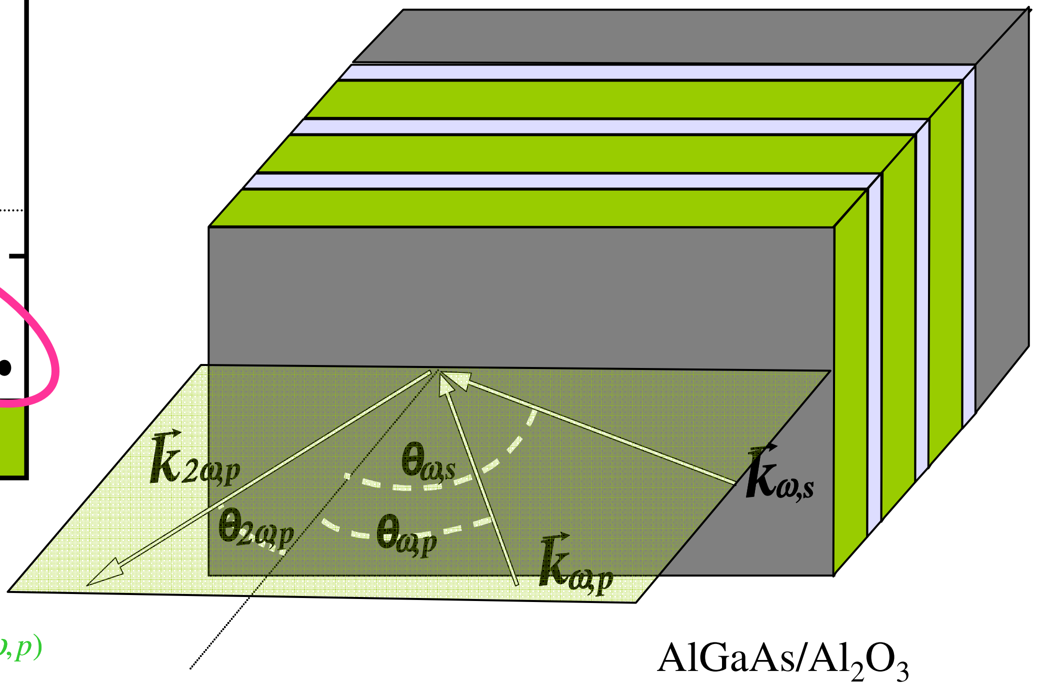

$AlGaAs/Al_2O_3$

λp=1.55 microns

Angular measurements:

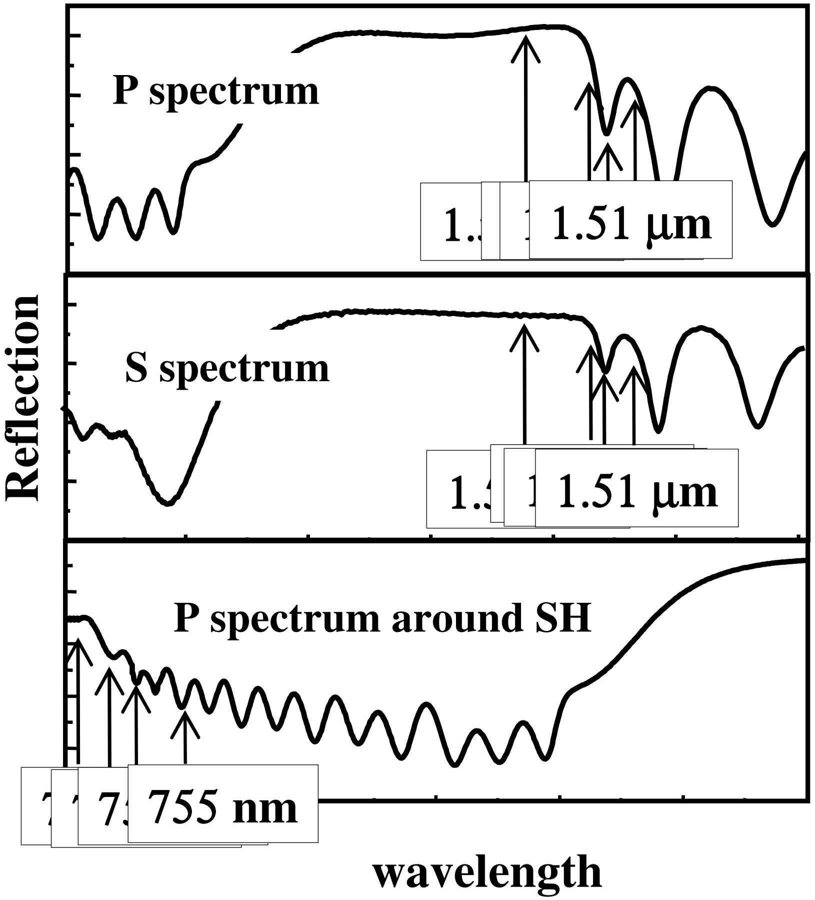

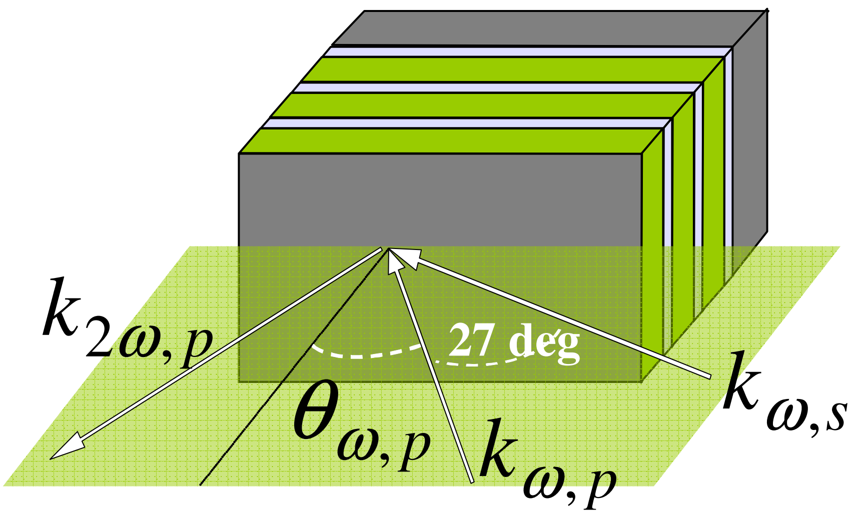

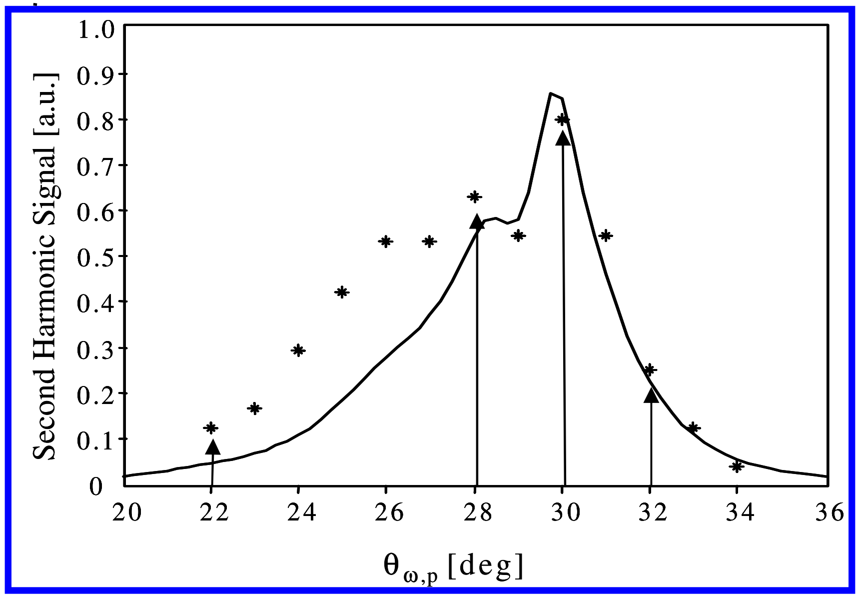

Almost no energy inside the photonic crystal

A. Bosco et al. Appl. Phys. Lett. 84, 3010 (2004).

Y. Dumeige et al APL 2001, JOSAB 2002

Y. Dumeige et al PRL 89, 043901 (2002)

Giant second-harmonic generation in a one-dimensional GaN photonic crystal

J. Torres, D. Coquillat,* R. Legros, J. P. Lascaray, F. Teppe, D. Scalbert, D. Peyrade, Y. Chen, O. Briot, M. Le Vassor d'Yerville, E. Centeno, D. Cassagne, and J. P. Albert

Groupe d'Etude des Semiconducteurs, UMR 5650, CNRS-Université Montpellier II, pl. E. Bataillon, 34095 Montpellier, France

and Laboratoire de Photonique et des Nanostructures, CNRS UPR 20, Route de Nozay, 91460 Marcoussis, France

(Received 8 July 2003; revised manuscript received 8 October 2003; published 20 February 2004)

PHYSICAL REVIEW B **69**, 085105 (2004)

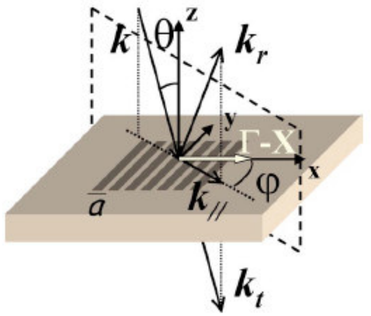

FIG. 1. Schematic diagram illustrating the 1D GaN PhC in planar waveguide geometry, and the coordinate system used in this study. Here a is the periodicity of the PhC.

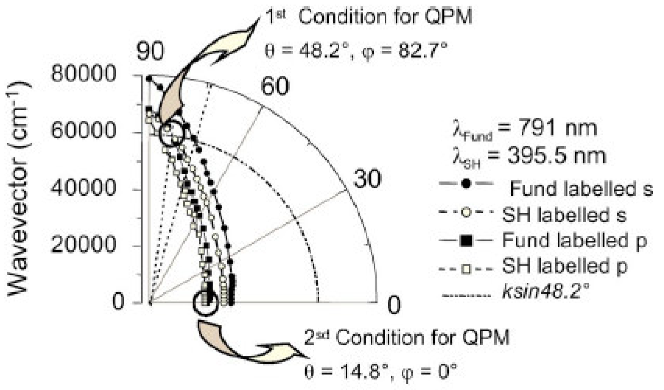

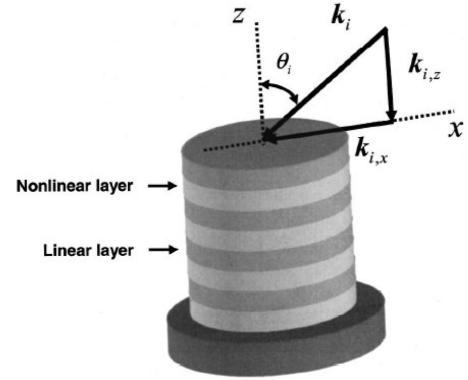

Fig. 1. Geometry of the PC studied. The incident wave vector and the incident angle are represented with respect to the two characteristic axes (x, z). The incident wave vector $\mathbf{k}_i$ is expanded into two orthogonal projections $(\mathbf{k}_{i,x}, \mathbf{k}_{i,z})$ related to the symmetry of the structure.

$$I_2^T \approx N^6$$

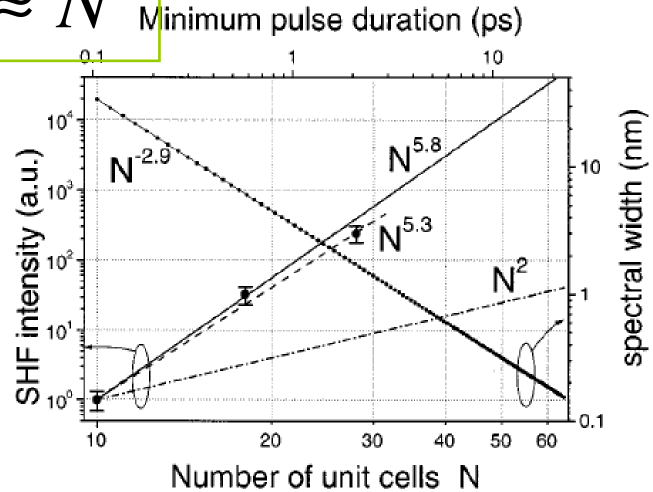

Fig. 9. SHF intensity, normalized to the value of the 10-period sample, plotted as a function of the number of PC unit cells N. The circles and the dashed curve correspond to the experimental results and the best fit, respectively. The solid curve is the theoretical prediction, whereas the usual quadratic law is represented by the dotted–dashed curve for comparison. The dotted curve is the calculated spectral width of the FF transmission resonance.

Optics Express, Vol. 14, Issue 25, pp. 12353-12358 (2006)

Simultaneous perfect phase matching for second and third harmonic generations in ZnS/YF_3 photonic crystal for visible emissions

Weixin Lu, Ping Xie, Zhao-Qing Zhang, George K. L. Wong and Kam Sing Wong*

Department of Physics, Hong Kong University of Science and Technology, Clear Water Bay, Hong Kong, P. R. China
* phkswong@ust.hk

Abstract: Theoretically designed and experimentally realized simultaneous perfect phase matching of second and third harmonic generations were demonstrated in a one-dimensional ZnS/YF_3 photonic crystal (PC) structure. Dramatic enhancement of second harmonic generation (SHG) and third harmonic generation (THG) in forward and backward directions near the photonic band edge were observed. This enhancement came from a combination of large ZnS nonlinear susceptibility coefficients, high density of optical modes and perfect phase matching of the fundamental and the harmonic waves near the photonic band edge due to modification of the dispersion curve by the PC structure. Total SHG and THG conversion efficiency over 4% is measured in only six micrometers length of photonic crystal. Theoretical calculations show good agreement with experimental measurements.

OCIS codes: (190.2620) Frequency conversio
(190.4360) Nonlinear optics devices.

M. Centini, et al,
"Simultaneously phase-matched enhanced second and third harmonic generation,"
Phys. Rev. E 64, 046606 (2001)

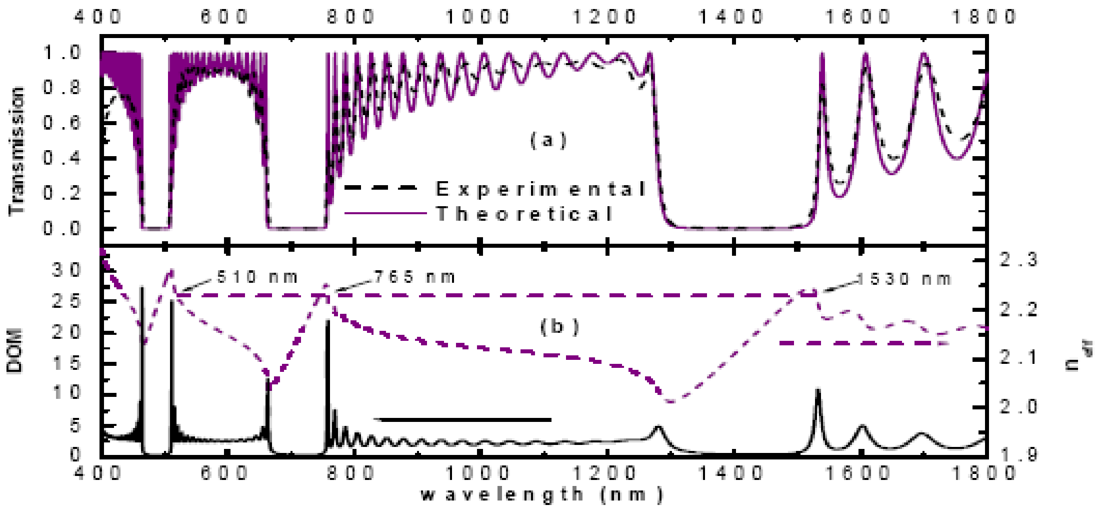

Fig. 1. (a) The experimentally measured (dotted line) and the corresponding theoretically calculated (solid line) transmission. (b) Effective refractive index (solid line) and density of modes (DOM) (dashed line) as a function of wavelengths of the same PC.

TWIN PHOTON GENERATION

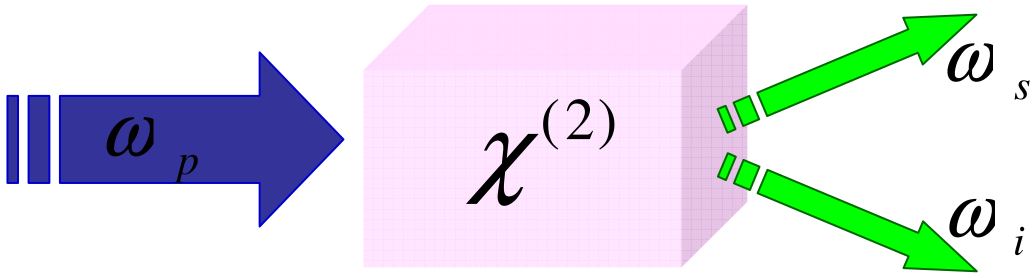

$$\omega_p = \omega_s + \omega_i;$$

$$\vec{k}_p = \vec{k}_s + \vec{k}_i$$

BULK MATERIAL

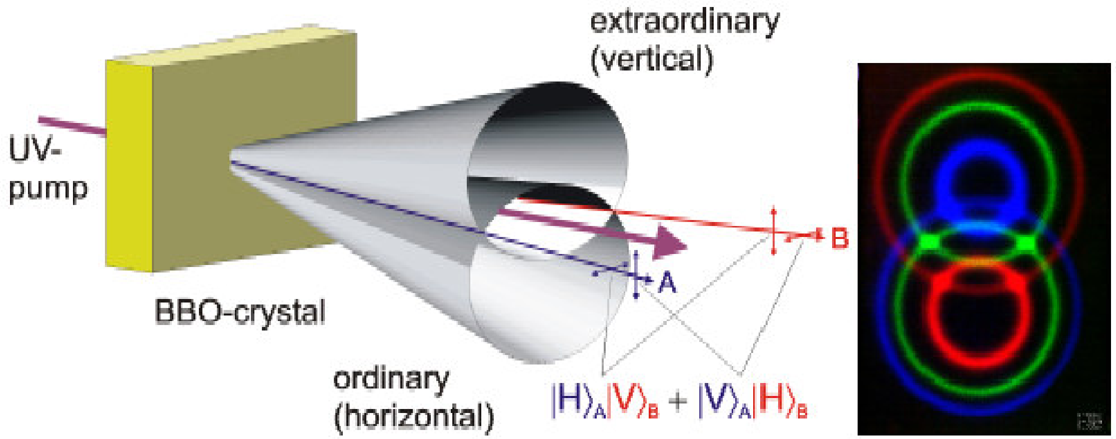

Kwiat et al. PRL 75 4337 (1995)

- Low efficiency
- Size
- Spatial and frequency filtering needed

TWIN PHOTON GENERATION In PhC

1D Ph Crystal

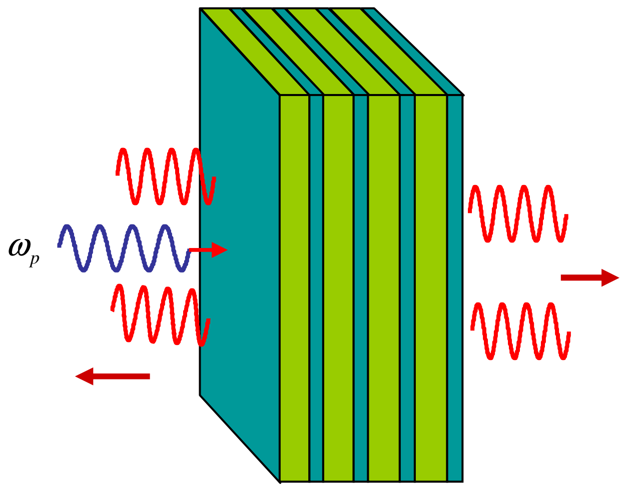

$$E_n = A_n^{(+)}(z)\Theta_n^{(+)}(z\ ) + A_n^{(-)}(z)\Theta_n^{(-)}(z\ )$$

✓Size
✓High brightness per mode
✓Narrow linewidth

Drawbacks:

Difficult to find suitable materials in the visible.

Single photon detection at 1500 nm is not as well developed and efficient as in the visible range.

Parametric Fluorescence

N=15of Al(30%)GaAs (160nm)/Al_2O_3(97nm)/ GaAs

Frequency degenerate emission:
30 deg p-pol 1510 nm and 57 deg s-pol 1510 nm

Non degenerate emission
30 deg s-pol 1550 nm e 57 deg p-pol 1470 nm

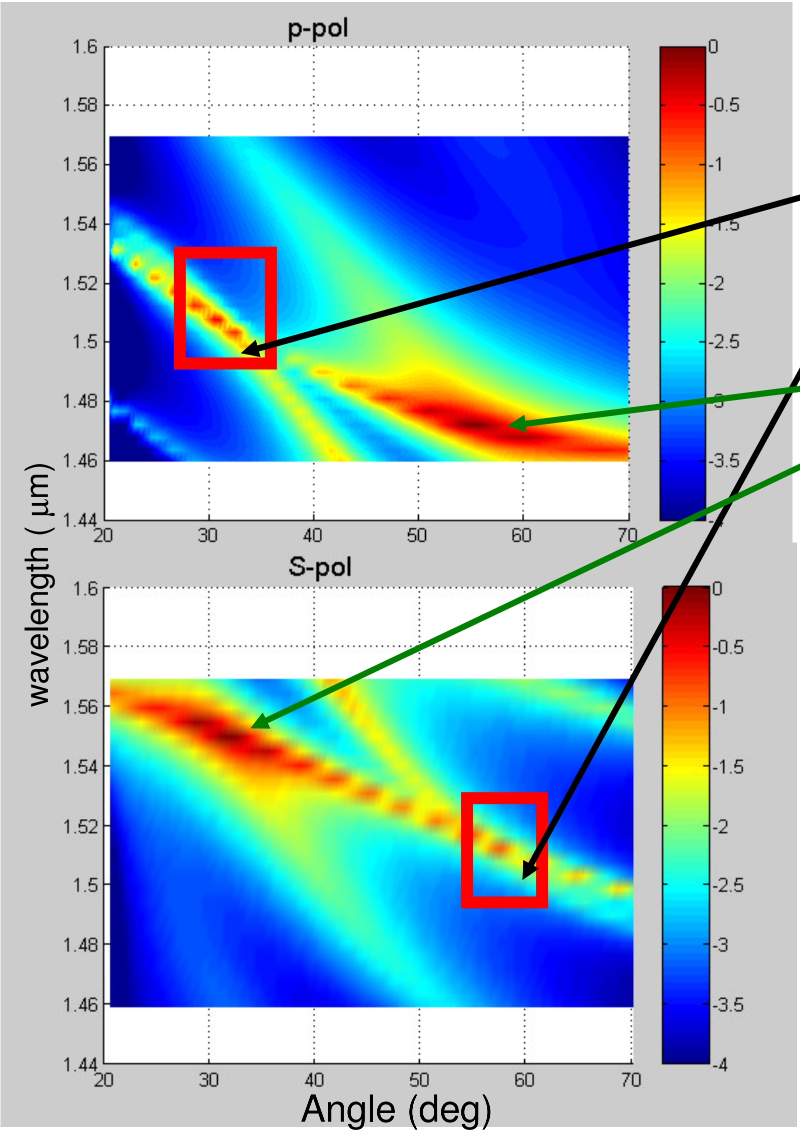

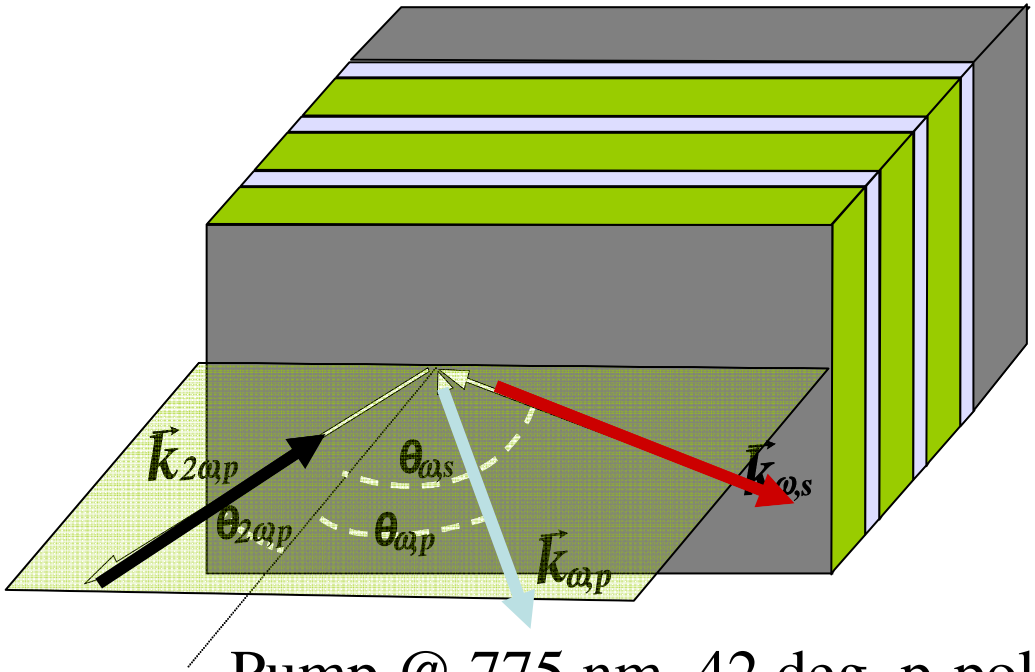

Pump @ 775 nm, 42 deg, p-pol

Centini et al. PRA 72, 033806 (2005)

J. Peřina Jr. et al. PRA 73, (2006)

Acknowledgements

Colleagues and collaborators in Rome:

Prof. Mario Bertolotti

Prof. Concita Sibilia

Dr. Mariacristina Larciprete

Dr. Alessandro Belardini

Dr. Letizia Sciscione

Dr. Michael Scalora
Dr. Giuseppe D'Aguanno
Charles M. Bowden Research Facility,
Bldg.7804, Redstone Arsenal, AL 35898-5000

Prof. Joseph W. Haus
Electro-Optics Program
University of Dayton, Dayton, OH 45469

Dr. Jan Perina jr.
Joint Laboratory of Optics of Palacky University and Institute of Physics of Academy of Sciences of the Czech Republic
Olomouc, Czech Republic.